

## Safe Estimation of Vehicle Side-slip for an Autonomous Heavy Vehicle

Master's thesis in Systems, Control and Mechatronics

PRANAY KOTUR



MASTER'S THESIS IN SYSTEMS, CONTROL AND MECHATRONICS

Safe Estimation of Vehicle Side-slip for an Autonomous Heavy Vehicle

PRANAY KOTUR

Department of Mechanics and Maritime Sciences  
Division of Vehicle Engineering and Autonomous Systems  
CHALMERS UNIVERSITY OF TECHNOLOGY

Göteborg, Sweden 2019

Safe Estimation of Vehicle Side-slip for an Autonomous Heavy Vehicle  
PRANAY KOTUR

© PRANAY KOTUR, 2019

Master's thesis 2019:99  
Department of Mechanics and Maritime Sciences  
Division of Vehicle Engineering and Autonomous Systems  
Chalmers University of Technology  
SE-412 96 Göteborg  
Sweden  
Telephone: +46 (0)31-772 1000

Cover:

Top left: Cross section of a Volvo truck during winter testing. Top right: Simulink block for the linear bicycle model used in the thesis. Bottom right: Visualization of a semitrailer truck showing roll, pitch and yaw axes. Bottom left: Measured sideslip lying between the estimated bounds.

Chalmers Reproservice  
Göteborg, Sweden 2019

Safe Estimation of Vehicle Side-slip for an Autonomous Heavy Vehicle

Master's thesis in Systems, Control and Mechatronics

PRANAY KOTUR

Department of Mechanics and Maritime Sciences

Division of Vehicle Engineering and Autonomous Systems

Chalmers University of Technology

## ABSTRACT

Stabilizing the lateral movement of the vehicle is crucial for functional safety. The variables required to ensure lateral stability cannot directly be measured from the vehicle. Hence, data from sensors is coupled with the estimates from the state estimator to obtain reasonably good estimates with a fair amount of accuracy. This technique called Sensor Fusion, helps to iteratively eliminate any outliers or anomalies and obtain the desired estimates.

In this thesis, three different models of state estimators were developed in MATLAB/Simulink and their results compared. Their accuracy was compared to select the best model which would estimate the side-slip correctly. Each of the models has been given bounds (i.e., a minimum and a maximum bound) for values of side-slip. These bounds were based on tire wear-and-tear and other tire parameters which would simulate the real-world experiences. So the main goal was to design the estimator such that the bounds would encompass the actual measured value from the sensors (also called as 'ground truth').

The first model used was based on the linear bicycle model given in lateral dynamics. This was basically a mathematical model with a given set of equations along with vehicle parameters and variables. For vehicles with simple configurations (i.e., passenger cars and rigid-body trucks) whose lateral behaviour is relatively simpler compared to multi-axle or multi-trailer vehicles, the linear bicycle model gives reasonably accurate estimates as long as the sideslip angle doesn't exceed 0.5 degrees . The second method used was the kinematics model which integrated the lateral acceleration to give lateral velocity, which in turn was used to compute side-slip. However, as is present with most integrators, this methods suffers from what is called as integration drift. The third and final model was a washout filter model which was effectively a combination of a high-pass (HP) and a low-pass (LP) filter. Lateral velocities from both the bicycle model as well as the kinematic model act as inputs for this filter. This filter retains decent accuracy even for high values of side-slip and is not prone to the errors which the above-mentioned models suffer from.

**Keywords:** side-slip angle, state estimator, tractor-semitrailer, lateral stability

## ACKNOWLEDGEMENTS

I would like to take this opportunity to profusely thank the people who have directly or indirectly helped me achieve the completion of this master thesis project.

First and foremost, I would like to thank my supervisors Mats Jonasson and Vinzenz Bandi for their constant support, valuable inputs and helping me solve even the most trivial of hurdles.

I would like to thank my examiner Leo Laine for his time, advice and patience, and for helping me out in any possible way he could.

I would like to thank my Master Program Coordinator Knut Åkesson for offering me this opportunity to work on this thesis.

Special thanks to Niklas Fröjd for his inputs on tire parameters, and Bengt Jacobson for his help on the semitrailer combination.

Finally, I would like to acknowledge my parents and sister who gave me invaluable advice on how to write a thesis report and their constant guidance and unwavering support. I would also like to thank all my friends without whose support and motivation, I would not have completed this thesis alone.

Gothenburg, October 2019

Pranay Kotur

# CONTENTS

<b>Abstract</b>	i
<b>Acknowledgements</b>	ii
<b>Contents</b>	iii
<b>1 Introduction</b>	1
1.1 Background . . . . .	1
1.2 Objective . . . . .	1
1.3 Assumptions and limitations . . . . .	2
1.4 Structure of the report . . . . .	2
<b>2 Theory</b>	3
2.1 Vehicle sideslip angle . . . . .	3
2.2 Sensor configuration . . . . .	4
2.3 Vehicle modelling . . . . .	5
2.3.1 Coordinate frame for vehicle and the RT3000 . . . . .	6
2.4 Road-tyre interaction . . . . .	7
2.5 Lateral acceleration . . . . .	8
<b>3 Functional Safety</b>	9
3.1 Definition . . . . .	9
3.2 The ISO 26262: Road Vehicles - Functional Safety Standard . . . . .	9
3.2.1 Background . . . . .	9
3.2.2 Goals . . . . .	10
3.2.3 Key components of the ISO 26262 Safety Standard . . . . .	10
3.2.4 Automotive Safety Integrity Level (ASIL) . . . . .	10
3.2.5 Risk and Hazard Assessment using ASIL . . . . .	11
<b>4 Vehicle Modelling for Estimating Side-slip</b>	13
4.1 Tyre model . . . . .	13
4.2 Complete vehicle model . . . . .	14
4.2.1 Equations of motion for vehicle . . . . .	14
<b>5 Methods for side-slip estimation</b>	18
5.1 Kinematic observer based on the linear bicycle model . . . . .	18
5.1.1 Estimating side-slip from the bicycle model . . . . .	18
5.2 Side-slip estimation by integrating lateral acceleration . . . . .	18
5.3 Washout filter method . . . . .	20
<b>6 Implementation</b>	21
6.1 Estimator using the bicycle model . . . . .	21
6.2 Model using the integration method . . . . .	21
6.3 Implementation of the washout filter . . . . .	22
<b>7 Results and Analysis</b>	24
7.0.1 Steady state steering with small constant radius . . . . .	24
7.1 Steady state steering with large constant radius . . . . .	26
7.2 Sinusoidal steering (slalom) manoeuvre . . . . .	28

<b>8 Conclusion and future work</b>	<b>31</b>
8.1 Approach . . . . .	31
8.2 Implementation . . . . .	31
8.3 Accuracy . . . . .	31
8.4 Errors and noise in measurement data . . . . .	32
8.5 Robustness . . . . .	32
8.6 Parameter identification . . . . .	32
<b>References</b>	<b>33</b>

# 1 Introduction

## 1.1 Background

Loss of control of the vehicle is one of the largest factors (about one third) when it comes to accidents [1]. Heavy vehicles, such as trucks, have a life, counted in covered distance, typically 10 times that of passenger cars. They have a much higher Centre of Gravity (CoG) as compared to lighter vehicles, can have multiple steered axles, carry heavy loads, and have smaller lateral margins in driving lanes. Hence there is a rising need for modern vehicles to adhere to a functional safety standard, especially heavy vehicles. The safety system of the vehicle should therefore be equipped to properly handle all possible scenarios such as human error, hardware failure or external/environmental factors.

In modern heavy-duty trucks, there exist many functions which require information about the current state of the vehicle for use in safety systems such as Electronic Stability Control (ESC), Anti-lock Braking System (ABS), etc. For such vehicular functions, it is necessary to have access to both the longitudinal as well lateral movement of the vehicle. This movement can be gauged or analyzed using the longitudinal as well as lateral components of velocities and accelerations.

One such parameter is the vehicle side-slip angle. For the purpose of vehicle dynamics, the vehicle side-slip is the angle between the forward velocity vector  $v_x$  and the vector sum of wheel forward velocity and lateral velocity [2]. This is illustrated below:

$$\beta = \arctan\left(\frac{v_y}{|v_x|}\right) \quad (1.1)$$

This differs from the tyre side slip angle which is typically the angle between tyre longitudinal direction and the tyre translational velocity. The side-slip gives us a measure of how much a vehicle skids and hence is an important parameter required to control the lateral stability and is vital for vehicular control such as braking control, stability control, motion planning, etc. In real-world applications, side-slip is typically difficult to measure by an Inertial Measurement Unit (IMU), which generally measures quantities such as angular speeds, angular accelerations, yaw rate, etc. Side slip measurement requires expensive instruments such as optical correlation sensors [3].

In this thesis, the reference measurement system used for collecting sensor data is called the *RT3000*, an Inertial and GPS Measurement System by Oxford Technical Solutions Limited which uses mathematical algorithms developed for use in aircraft navigation systems, to obtain high-precision measurements [4].

For the purpose of the report, it is assumed that the reader is familiar or well-versed with the basic concepts in Lateral Vehicle Dynamics.

## 1.2 Objective

The objective of this thesis is to design a state estimator (also called as observer) for the estimation of vehicle lateral slip (called side-slip and denoted by  $\beta$ ) such that the measured values of side-slip, obtained from sensors in the vehicle, lie between the given bounds for minimum and maximum values of side-slip. The bounds for the min. and max. side-slip are set after considering the various parameters affecting the side-slip in real time such as change in cornering stiffness of tyre due to wear and typical tread depth wear-out.

The estimator designed aims to be applicable for a tractor-semitrailer combination in addition to rigid-body vehicles.

### 1.3 Assumptions and limitations

The concepts discussed in this thesis report are an extension of methods already existing for use in passenger cars, with appropriate modifications required to be applicable to heavy trucks. The methods discussed need to be developed further to actually be implemented in production trucks.

Some of the parameters assumed to be known are:

- Total mass of the vehicle.
- Yaw moment of inertia.
- Front and rear tyre stiffness.
- Wheelbase and track width of the vehicle.
- Effective wheel radius, maximum tyre radius, minimum tyre radius.

The following variables are assumed to be available from the sensors in the vehicle:

- Front road-wheel angle.
- Yaw rate of the vehicle.
- Longitudinal as well as lateral acceleration of the vehicle.
- Angular velocities of all the wheels.

Below are listed some of the limitations of the estimator approach used in this thesis project:

- A linear bicycle model is used for the tractor semitrailer combination as modelling the equations for transient dynamics for such a combination proved to be costly to solve.
- The road surface is assumed to be flat with no angle of banking.

### 1.4 Structure of the report

The thesis report is divided into five chapters. The first chapter is the introduction. The second chapter discusses the different methods for side-slip estimation. The third chapter discusses the implementation and verification of the methods. Chapter 4 discusses the results and their analysis and the final chapter concludes the findings of this master thesis along with possibilities of future work.

## 2 Theory

Most modern vehicles are equipped with electronic control systems, that help mitigate the risk of accidents. For example, most vehicles generally have an anti-lock braking system (ABS), which prevents the locking of wheels during braking, or an electronic stability control system (ESC), which prevents skidding by stabilizing the vehicle's lateral motion. Front Collision Warning (FCW) systems, Collision Avoidance systems, rollover prevention, are some other examples of electronic control systems present in vehicles for safety. [3].

Such systems rely on information about the vehicle's condition and its environment. Modern vehicles are fitted with different sensors to obtain this data. For a typical vehicle with ESC, the measurements needed include the angle of the steering wheel, road-wheel angle, angular velocities of the wheel, lateral acceleration, and yaw rate. These measurements contain a lot of information about vehicle's state. The vehicle speed can be estimated using angular velocities of the wheels and road-wheel angle. Other measurements taken as inputs can be used to predict the vehicle behaviour under both normal and critical driving conditions. This estimated behaviour can then be compared with the actual vehicle behaviour (called ground truth).

While some quantities are easily measurable, others are difficult to measure because of computational complexity, high cost or simply because it is impractical to measure these quantities directly. When some quantity cannot be directly measured, it is often more practical to estimate it using the other available measurements. State observers combine the measurements that are available with dynamic models to estimate unknown states. The dynamic models in question, need to be carefully constructed to ensure sufficient accuracy of the entire system.

### 2.1 Vehicle sideslip angle

When the vehicle is driven on a level surface, the orientation of the vehicle's longitudinal axis and the CoG's direction of travel coincide. However, when the vehicle is turning, the orientation changes, and an acceleration in the lateral direction of the vehicle directed towards the center of the turning arc is observed because the vehicle exhibits a yaw rate. A lateral velocity component is also seen, which means that the direction of travel and the orientation of the vehicle are no longer the same. Since the lateral velocity varies from point to point on the vehicle body, the vehicle's CoG is considered as a reference point to measure lateral velocity. All variables, along with the forces acting on the vehicle are illustrated in the Figure 2.1. given below.

The vehicle sideslip angle is defined as the angle between the center line of the vehicle and the direction of travel at the CoG. For an arbitrary point in the vehicle, it is defined as:

$$\beta = \arctan\left(\frac{v_y}{|v_x|}\right) \quad (2.1)$$

where  $v_y$  is the lateral velocity and  $v_x$  is the longitudinal velocity of the vehicle. In production trucks, the vehicle sideslip angle is not measured by the inbuilt Inertial Measurement Unit (IMU), because measuring sideslip requires expensive equipment. When the vehicle is driven without the risk of losing road grip (under normal driving conditions), the vehicle sideslip angle is small, not exceeding  $\pm 2^\circ$  [5]. For a given speed under normal driving situations, there exists an interconnection between the lateral acceleration, road-wheel angle, yaw rate, and vehicle sideslip angle.

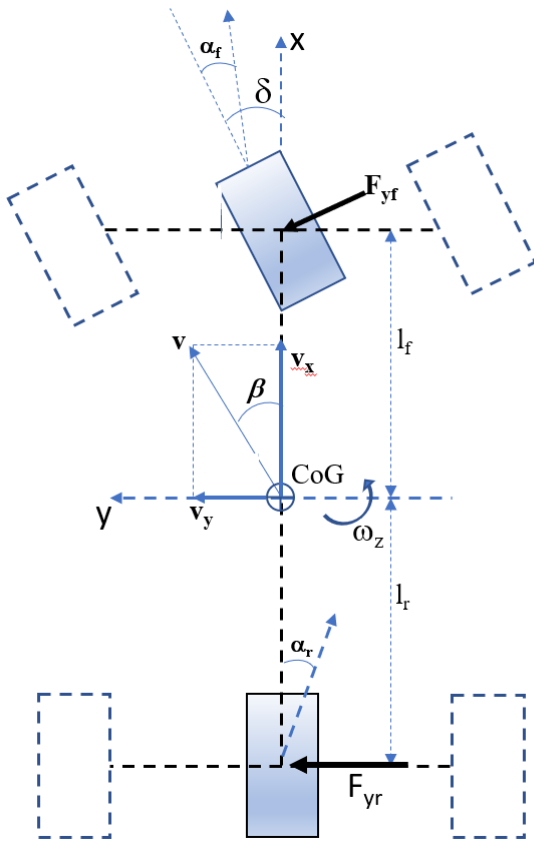


Figure 2.1: Figure showing all the variables, including forces [6]

The vehicle sideslip angle can therefore be estimated using a steady-state model or a simple linear model. In critical driving conditions, however, when the vehicle's friction limits between the tyres and the road surface are tested, the vehicle displays highly nonlinear behaviour due to the non-linearity of the friction forces between the tyres and the road surface. In situations like these, the vehicle sideslip angle can become quite large, and for a proper description of vehicle behavior, sufficient knowledge about the sideslip is required .

## 2.2 Sensor configuration

Choice of sensor configuration is a crucial design consideration in estimation problems. Most automotive-grade sensor configurations primarily aim to cut costs, which often translates into sensors with low resolution, limited range, substantial bias, drift and noise. The quality of sensors puts fundamental constraints on the accuracy that can be expected from any estimator design. In inertial sensors, drift and bias are particularly limiting, because they hinder accurate integration of kinematic equations over long time spans.

Most standard sensor configurations found in modern vehicles consist of an Electronic Stability Control (ESC) system. The ESC incorporates yaw rate control into the anti-lock braking system (ABS) found in modern vehicles. Anti-lock brakes enable ESC to slow down individual wheels. Many ESC systems also incorporate a traction control system (TCS), which senses drive-wheel slip under acceleration and individually brakes the slipping wheel or wheels and/or reduces excess engine power until control is regained. The ESC system uses several sensors to determine where the driver intends to travel. Other sensors indicate the actual state of the vehicle. The control algorithm compares driver input to vehicle response and decides, when necessary, to apply brakes and/or reduce throttle by the amounts calculated through the state space (set of equations used to model the dynamics of the vehicle) [5]. GPS navigation systems are not yet standard equipment, even

in the latest production vehicles, even though GPS measurements would add important information to the above-mentioned measurements. Also, GPS signals are sometimes degraded or weak, especially when driving under bridges or tunnels or any other large structures. In addition, ESC-type sensors may suffer from significant sensor drift and bias, which places constraints on designs which rely mainly on kinematic equations.

It is because of this reason, that a special reference measurement system called the *RT3000*, which has been mentioned previously, is used to log measurement data [4].



Figure 2.2: The *RT3000* Inertial and GPS Measurement System.

The *RT3000* is a combination of an Inertial Measurement Unit (IMU) and a GPS Measurement System. The inertial block consists of three accelerometers and three gyroscopes, while measurements from high-grade GPS receivers update the position and velocity navigated by the inertial sensors [4]. This innovative approach of combining the data from two separate blocks within the *RT3000* give it the following advantages over systems that use GPS alone:

- The *RT3000* has a high 100 Hz update rate and a wide bandwidth.
- The outputs are available with very low, 3.9ms latency.
- All outputs remain available continuously during GPS blackouts when, for example, the vehicle drives under a bridge.
- The *RT3000* recognises jumps in the GPS position and ignores them.
- The position and velocity measurements that the GPS makes are smoothed to reduce the high-frequency noise.
- The *RT3000* makes many measurements that GPS cannot make, for example acceleration, angular rate, heading, pitch, roll, etc.

It must, of course, be noted that systems like the *RT3000* are not standard equipment for production vehicles, and for the scope of this thesis project, a vehicle specially fitted with this system has been used to log only the necessary data such as measured side-slip.

Most production vehicles have an inbuilt IMU for logging data such as angular speeds and accelerations. The vehicle used for logging data for the purpose of this thesis was a test vehicle, with additional sensors and measurement systems (including the *RT3000*) fitted on to its frame as well as inside the cabin. Specifically, it has two additional IMUs, data from which (namely parameters such as lateral acceleration, individual wheel speeds and the road-wheel angle) has been used to serve as inputs for the purpose of sideslip estimation.

## 2.3 Vehicle modelling

Vehicle models usually comprise of a model of the road-tyre friction forces. The inherent uncertainty that comes along is the main argument against using such models. Unknown variations are introduced in the model, for example, due to variations in vehicle mass and the tyre characteristics.

The main measurement equation comes from the longitudinal velocity, which is estimated separately based

primarily on the wheel speeds. This idea is similar to the kinematic observer approach listed under methods in chapter 4. These type of designs are sensitive to sensor drift (also called integration drift) as well as sensor bias. This sensitivity could also be due to misalignment of the sensor cluster. Sensor bias is defined as a constant error in the measurement signal, whereas drift is defined by a slowly varying error which accumulates over time, either due to numerical integration of particular quantities or due to the gravity component being present. Inertial sensor drift is mainly caused by changes in temperature [7].

For a vehicle driving on a flat surface, the longitudinal and lateral velocities at the centre of gravity (CoG) are given by the equations of motion listed below:

$$\dot{v}_x = a_x + \omega_z v_y \quad (2.2)$$

$$\dot{v}_y = a_y - \omega_z v_x \quad (2.3)$$

where  $v_x$  and  $v_y$  are the longitudinal and lateral velocities,  $a_x$  and  $a_y$  are the longitudinal and lateral accelerations, and  $\omega_z$  is the yaw rate. Each of the equations given by (2.2), (2.3) include an acceleration term and a yaw rate term  $\omega_z$ . The accelerations are attributable mainly to road-tyre friction and hence, are directly related to the forces acting on the vehicle. The yaw rate terms appear because the coordinate system in which the velocities and accelerations are resolved is fixed to the vehicle, which rotates with respect to an inertial coordinate system. The vehicle is illustrated in Figure 2.3, where the velocities, the yaw rate are alongside sideslip angle  $\beta$ .

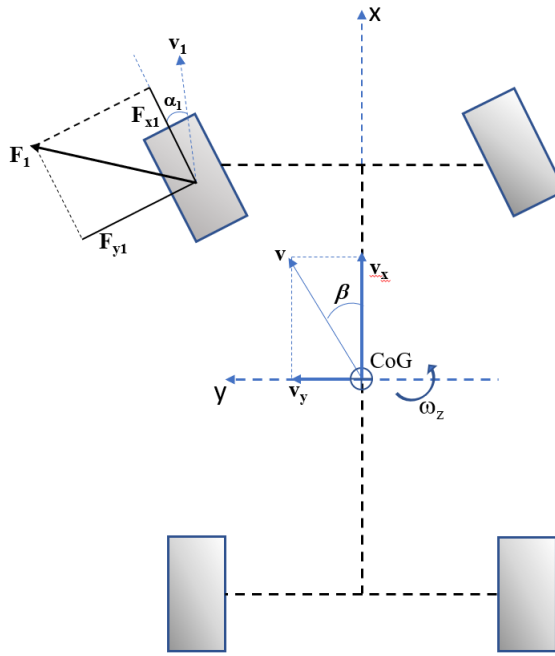


Figure 2.3: Illustration of the vehicle model along with forces acting on one wheel.

### 2.3.1 Coordinate frame for vehicle and the RT3000

The equations of motion for the vehicle are usually described in coordinate system called the *vehicle coordinate frame* [8]. This coordinate system has its origin at the CoG of the vehicle. The orientation of the vehicle is then described according to an earth-fixed coordinate system called the *global coordinate frame*.

In this thesis project, the *vehicle coordinate frame* is defined as per ISO standard 8855 [8]. It has the *x-axis* pointing forward, in the longitudinal direction of the vehicle, the *y-axis* pointing left relative to the position of the driver and the *z-axis* pointing upwards.

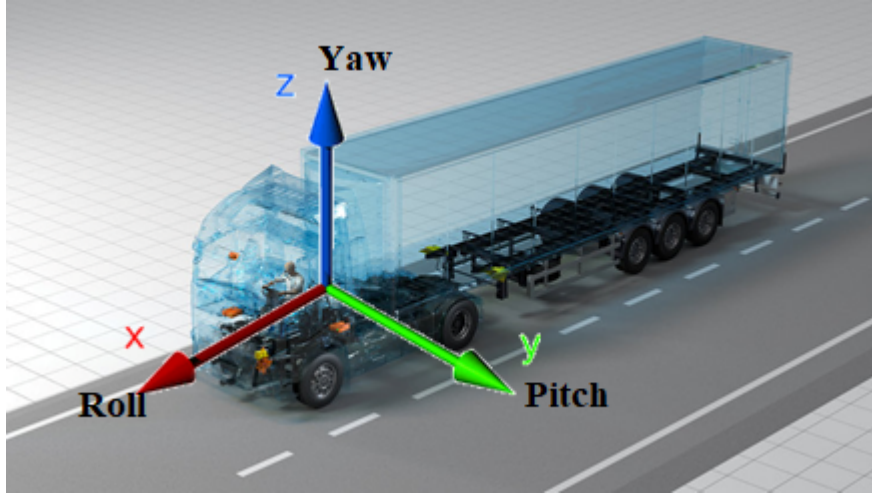


Figure 2.4: Vehicle Coordinate Frame Definition.

For the Inertial Measurement and GPS system, the RT3000, the axes are as follows: the *x-axis* is pointing forward in the longitudinal direction of the vehicle. the *y-axis* is pointing right relative to driver's position and the *z-axis* is pointing downwards [4]. In this thesis, the phase shift of  $180^\circ$  for the *y* and *z* axes is taken into

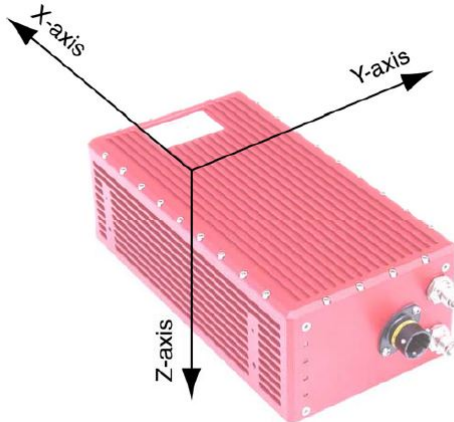


Figure 2.5: RT3000 Coordinate Frame Definition

account in calculations pertaining to side-slip estimation.

## 2.4 Road-tyre interaction

When the vehicle takes a turn, the vehicle's front tyres point in a different direction from the direction of travel, and we get what is called the tyre-slip angle. The tyre-slip angle is conceptually close to the vehicle sideslip angle. The only exception is that a single tyre, rather than the vehicle's entire body, is connected with the appropriate reference frame. By definition, the tyre-slip angle is the angle between the velocity vector at the wheel center and the tyre orientation.

This definition is illustrated in Figure 2.3, where  $\alpha_1$  denotes the tyre-slip angle for the front left wheel. In the lateral direction of the tyre, a non-zero tyre-slip angle means a relative difference in speed between the road surface and the tyre. Because the tyre is elastic, it doesn't just slip across the surface of the road. As a point on the tyre tread rolls into ground contact, its trajectory is deflected and it grips the surface for a short time. This mechanism contributes to the tyre's deformation, and the resistance of the tyre to this deformation produces lateral forces that cause the vehicle to turn. As the vehicle begins to turn, the rear tyres are also susceptible to the tyre-slip angles. After an initial transient, a stable steady state is reached in which the

road-tyre friction forces equilibrium to give the vehicle body zero net moment.

We also define the longitudinal tyre slip, as the normalized difference between the circumferential speed of the tyre and the speed of the wheel center along the direction of the tyre [9]. Longitudinal tyre slip gives rise to longitudinal friction forces, as illustrated in Figure 2.1 by  $F_{x1}$ . The longitudinal tyre slip can be expressed as:

$$s_x = \frac{R\omega - v_x}{|R\omega|} \quad (2.4)$$

$$s_x = \frac{R\omega - v_x}{|v_x|} \quad (2.5)$$

where R is the radius of the wheel in [m],  $\omega$  is the tyre angular velocity in [rad/s]. Equation 2.4 is often used for driven wheels and equation 2.5 is often used for braked wheels. This is to avoid division by a small denominator value in case of take-off and brake tests, respectively. Both the longitudinal tyre slip and the lateral tyre slip together are collectively known as the tyre slips. The friction forces between road and tyre are roughly linear in relation to the tyre slips during normal driving. But, in extreme situations such as polished ice or extremely wet roads, where the  $\mu$  friction coefficient is very small, the slips (both longitudinal and lateral) of the tyre may become so significantly large that this linearity is lost. The tyre loses road grip beyond a certain point and begins to slide across the surface of the road. In this case, the forces of road-tyre friction saturate, meaning an increase in the tyre slips does not result in a corresponding increase in the forces of friction.

## 2.5 Lateral acceleration

Newton's second law states that the vehicle's acceleration at the CoG in each direction is equal to the total force acting on the vehicle in that direction, divided by the mass ( $a = F/m$ ). When we are considering banked roads, rather than a horizontal road surface, gravity acts in the tangential plane of the road surface. This affects the vehicle velocity. It is assumed in the entire scope of this thesis that the road surface is horizontal. The dominant forces acting in the plane of the road surface are the road-tyre friction forces; we ignore smaller influencing factors such as wind resistance and air drag. The road-tyre friction forces are functions of the tyre slips  $s_x$  and  $s_y$ , which in turn are functions of the vehicle velocities  $v_x$  and  $v_y$  respectively. By kinematic relations, measurements of the vehicle accelerations depend on the vehicle velocities, and hence, the accelerations can be used for indirect measurements of the vehicle velocities. In particular, the lateral acceleration  $a_y$  contains vital data about the lateral velocity. The algebraic relations are shown through the following equations [9]:

### Road-tyre friction forces

$$F_x = C_x s_x \quad (2.6)$$

and

$$F_y = -C_y s_y; \quad s_y = \frac{v_y}{|R\omega|} \quad (2.7)$$

where  $s_x$  is defined by equations 2.4 and 2.5 mentioned previously.  $C_x$  and  $C_y$  are called the "longitudinal tyre stiffness" and the "tyre cornering stiffness" respectively. We can define the "longitudinal tyre (slip) stiffness"  $C_x$ , which has the unit N as the derivative of force with respect to slip at slip  $s_x = 0$ . The "tyre cornering stiffness" or "lateral tyre slip stiffness"  $C_y$  can be similarly defined for  $s_y = 0$ :

$$C_x = \left( \frac{\partial F_x}{\partial s_x} \right) \Big|_{s_x=0}; \quad C_y = - \left( \frac{\partial F_y}{\partial s_y} \right) \Big|_{s_y=0}; \quad (2.8)$$

The longitudinal tyre slip stiffness  $C_x$ , is normally larger than the lateral tyre slip stiffness  $C_y$ , which can be explained with the fact that the tyre is less stiff in the lateral direction. **Lateral acceleration**

$$a_y = \frac{1}{m} \sum_{i=1}^N \sum_{j=1}^2 (F_x \sin(\delta_{ij}) + F_y \cos(\delta_{ij})) \quad (2.9)$$

where N is the number of axles of the vehicle and  $\delta_{ij}$  is the steering angle of the front wheels [10].

### 3 Functional Safety

#### 3.1 Definition

For any system, the functional safety is that part of overall safety which depends on automatic protection operating correctly in response to its inputs or failure in a fail-safe manner by responding appropriately to handle human errors, operational stress or hardware failure. In the context of this thesis, functional safety forms an integral part of each automotive product development phase, ranging from the specification, to design, implementation, integration, verification, validation, and production release. Hence, there is a need for an international safety standard which ensures uniformity globally. The ISO 26262 is an international standard for functional safety in production automobiles defined by the International Organization for Standardization (ISO) in 2011 [11].

#### 3.2 The ISO 26262: Road Vehicles - Functional Safety Standard

The ISO 26262 defines functional safety for automotive equipment applicable throughout the lifecycle of all automotive electronic and electrical safety-related systems. The ISO 26262 is an adaptation of the functional safety standard IEC 61508 [12], and like its parent standard, the 26262 is a risk-based safety standard, where the risk of hazardous operational situations is qualitatively assessed and safety measures are defined to avoid or control systematic failures and to detect or control random hardware failures, or mitigate their effects.

##### 3.2.1 Background

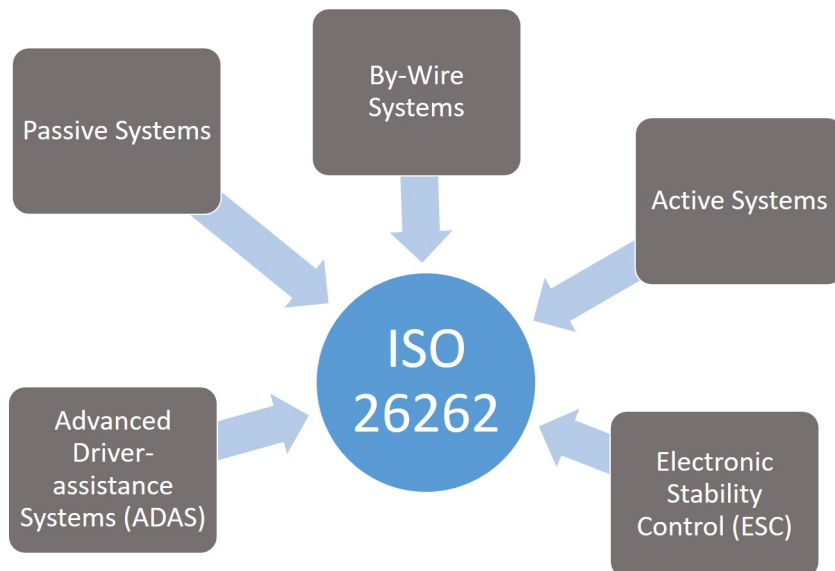


Figure 3.1: The different facets of the ISO 26262.

Increasing complexity throughout the automotive industry is resulting in increased efforts to provide safety-compliant systems. Therefore, the main goal of ISO 26262 is to provide a unifying safety standard for all automotive E/E systems.

The Draft International Standard (DIS) of ISO 26262 was published in June 2009. Because a public draft standard is available, the ISO 26262 is treated as technical state-of-the-art by law. The technical state-of-the-art is the highest development level of a product or process at a given time. Therefore, implementation of the ISO 26262 allows leveraging a common standard to measure how safe a system will be in service. It also provides the ability to reference specific parts of your system because of a common vocabulary provided by the standard.

This falls in line with other safety-critical application areas; a common standard provides a way to measure how safe a particular system is [13].

### 3.2.2 Goals

According to the International Organization for Standardization (ISO), the ISO 26262 standard has the following goals which it is meant to fulfill:

- Provides an automotive safety lifecycle (management, development, production, operation, service, decommissioning) and supports tailoring the necessary activities during these lifecycle phases.
- Covers functional safety aspects of the entire development process (including such activities as requirements specification, design, implementation, integration, verification, validation, and configuration).
- Provides an automotive-specific risk-based approach for determining risk classes (Automotive Safety Integrity Levels, ASILs).
- Uses ASILs for specifying the item's necessary safety requirements for achieving an acceptable residual risk.
- Provides requirements for validation and confirmation measures to ensure a sufficient and acceptable level of safety is being achieved.

### 3.2.3 Key components of the ISO 26262 Safety Standard

The ISO 26262 contains 10 key components:

1. Vocabulary.
2. Management of functional safety.
3. Concept phase.
4. Product development at the system level.
5. Product development at the hardware level.
6. Product development at the software level.
7. Production and operation.
8. Supporting processes.
9. Automotive Safety Integrity Level (ASIL)-oriented and safety-oriented analysis.
10. Guideline on ISO 26262.

For the purpose of this thesis, section 9 on ASIL analysis will be emphasized on in the following section.

### 3.2.4 Automotive Safety Integrity Level (ASIL)

The ASIL is a key component for ISO 26262 compliance. The ASIL is determined at the beginning of the development process. The intended functions of the system are analyzed with respect to possible hazards. The ASIL asks the question, “If a failure arises, what will happen to the driver and associated road users?” [13]

The estimation of this risk, based on a combination of the probability of exposure, the possible controllability by a driver, and the possible outcome’s severity if a critical event occurs, leads to the ASIL. The ASIL does not address the technologies used in the system; it is purely focused on the harm to the driver and other road users. ASIL has four levels, ASIL A, ASIL B, ASIL C and ASIL D, with D having the strictest testing regulations and the most safety critical processes. The ISO 26262 standard specifically identifies the minimum testing requirements depending on the ASIL of the component.

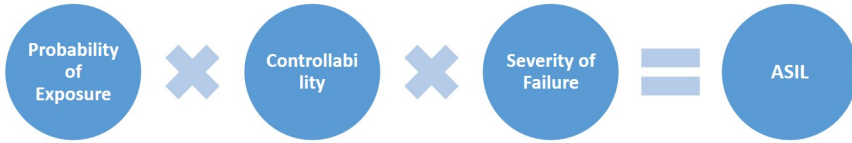


Figure 3.2: Risk Assessment using ASIL.

### 3.2.5 Risk and Hazard Assessment using ASIL

In the context of ISO 26262, each hazard is assessed in terms of severity of possible injuries within the context of how much of the time a vehicle is exposed to the possibility of the hazard happening as well as the relative likelihood that a typical driver can act to prevent the injury.

Risk may be generally expressed as:

$$\text{Risk} = (\text{expected loss in case of an accident}) \times (\text{probability of accident})$$

OR

$$\text{Risk} = \text{Severity} \times (\text{Exposure} \times \text{Likelihood})$$

Therefore, ASIL may be similarly expressed as:

$$\text{ASIL} = \text{Severity} \times (\text{Exposure} \times \text{Controllability})$$

as is illustrated by figure 3.2

Furthermore, the Severity, Exposure and Controllability Levels can be classified as follows:

#### Severity Levels (S)

- S0: No Injuries
- S1: Light to moderate injuries
- S2: Severe to life-threatening (survival probable) injuries
- S3: Life-threatening (survival uncertain) to fatal injuries

#### Exposure Levels (E)

- E0: Incredibly unlikely
- E1: Very low probability (injury could happen only in rare operating conditions)
- E2: Low probability
- E3: Medium probability
- E4: High probability (injury could happen under most operating conditions)

#### Controllability Levels (C)

- C0: Controllable in general
- C1: Simply controllable
- C2: Normally controllable (most drivers could act to prevent injury)
- C3: Difficult to control or uncontrollable

## **How are these classifications used to define ASIL?**

In terms of these classifications, an Automotive Safety Integrity Level D hazardous event (ASIL D) is defined as an event having reasonable possibility of causing a life-threatening (survival uncertain) or fatal injury, with the injury being physically possible in most operating conditions, and with little chance the driver can do something to prevent the injury. That is, ASIL D is the combination of S3, E4, and C3 classifications. For each single reduction in any one of these classifications from its maximum value (excluding reduction of C1 to C0), there is a single-level reduction in the ASIL from D. For example, a hypothetical uncontrollable (C3) fatal injury (S3) hazard could be classified as ASIL A if the hazard has a very low probability (E1). The ASIL level below A is the lowest level, Quality Management (QM). QM refers to the standard's consideration that below ASIL A; there is no safety relevance and only standard Quality Management processes are required [11].

## 4 Vehicle Modelling for Estimating Side-slip

### 4.1 Tyre model

Tyres are the only points of interaction between road and tyre. Therefore, the tyre forces arising due to contact are the only inputs when we consider the motion of the vehicle. There are primarily three types of forces acting on a tyre:

- The longitudinal tyre force, due to propulsion or braking,  $F_x$ .
- The lateral tyre force, due to cornering,  $F_y$ .
- The vertical tyre force arising due to vertical load transfer,  $F_z$ .

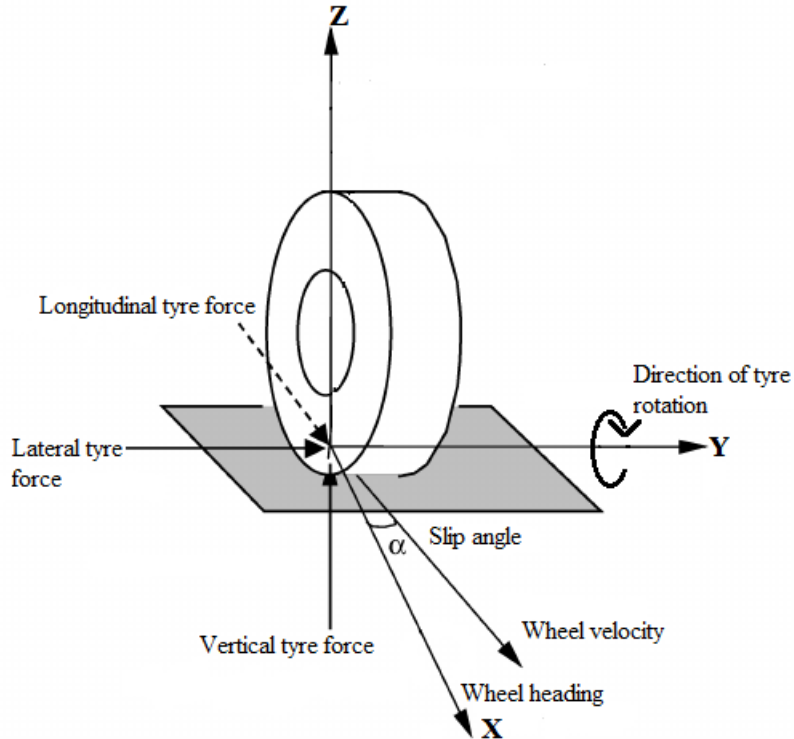


Figure 4.1: Forces acting on a tyre.

In addition to these forces, we consider two variables important for understanding how to model tyre forces: the wheel side-slip angle  $\alpha_{ij}$  and the angular wheel speed (velocity)  $\omega_{ij}$ , ( $i = 1, 2$ ;  $j = 1, 2$ ). All the forces and variables are depicted in figure 4.3 [14].

Tyre slips have been previously defined in section 2.4, which will be used to define the tyre model used in the scope of this thesis.

There exist many models which are used for describe the tyre forces, and each of these models have varying complexity and different levels of accuracy. Some of the existing models are the Pacejka "Magic Formula" model, Dugoff's tyre model and the Brush model.

However, for the purpose of this thesis, the **linear tyre model** has been used which is described in section 2.5.

We can see that these equations have been previously been well elaborated in section 2.5, where  $C_x$  and  $C_y$  represent the tyre cornering stiffnesses and  $s_x$ ,  $s_y$  represent the tyre slips. The choice of using the linear

tyre model was made keeping in mind the objective of having a model with as few parameters as possible, which has been shown to be valid over a wide slip range, and can be used in normal as well as critical driving conditions. The linear tyre model does well to achieve this objective.

Further details for other models mentioned above such as the Magic Formula model, Dugoff's model and Brush model have been published in [2], [15] and [9] respectively.

## 4.2 Complete vehicle model

### 4.2.1 Equations of motion for vehicle

There are two test cases that have been considered in the scope of this thesis. The first one is for the vehicle without a trailer, i.e., a rigid-body vehicle. The second case is for a tractor-semitrailer combination. The vehicle models have been expressed in state-space form. This form has two equations. The first equation, called the state equation describes the change in the state variables with respect to time as a direct result of the inputs, whereas the second equation, called the output equation, describes how the output varies as a result of the input.

#### Bicycle model without trailer

This model is based on certain approximations and assumptions [9]. It is based on a single-track geometry (hence the name "bicycle model"). It assumes a constant longitudinal velocity  $v_x$ , which is taken as an input along with the front road wheel angle  $\delta$ . It also assumes small steering and slip angles. The model also neglects effects such as lateral load transfer and body roll. The model is simple and hence computationally inexpensive, and can be used with nonlinear feedback methods.

The vehicle mass is taken as  $m$ . The distances of the front and rear axle from the CoG are taken as  $l_f$  and  $l_r$  respectively. The wheelbase of the truck is the sum of  $l_f$  and  $l_r$  and is denoted by  $L$ . The tyres are modelled with front and rear cornering stiffnesses denoted by  $C_{12}$  and  $C_{34}$  respectively. It must be noted that while the longitudinal and lateral forces on the tyre are denoted as  $F_x$  and  $F_y$  in previous chapters, here since we have more than one wheel in both the tractor-only model as well as the semitrailer combination, the different forces acting on each of the tyres are given subscripts (such as  $F_{fxw}$ ,  $F_{fyw}$ ,  $F_{ry}$ ,  $F_{1fxw}$ ,  $F_{1fyw}$ ,  $F_{1rx}$ ,  $F_{1ry}$ ,  $F_{2x}$ ,  $F_{2y}$ , where the subscripts 1,2 denote the 1<sup>st</sup> and 2<sup>nd</sup> units of the vehicle,  $f$  and  $r$  denote front and rear wheels,  $v$  and  $w$  denote forces with respect to vehicle frame or wheel frame). The same subscripts hold good for velocities as well.

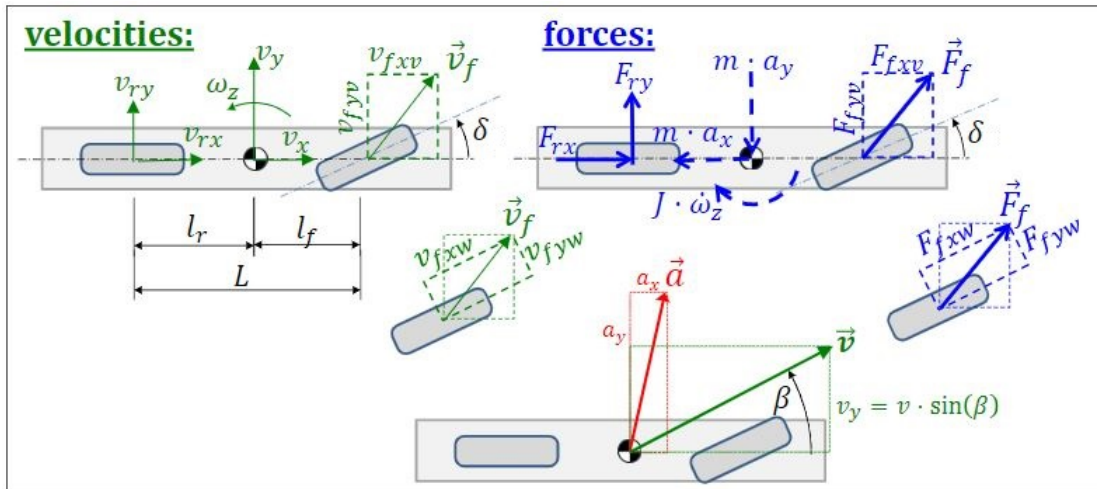


Figure 4.2: Bicycle model for transient dynamics. The dashed lines show fictive forces. Image Courtesy: Vehicle Dynamics Compendium, 2019 Edition [9].

**Equilibrium:**

$$\begin{aligned} m(\dot{v}_x - \omega_z v_y) &= F_{fxw}\cos(\delta) - F_{fyw}\sin(\delta) + F_{rx} \\ m(\dot{v}_y + \omega_z v_x) &= F_{fxw}\sin(\delta) + F_{fyw}\cos(\delta) + F_{ry} \\ J\dot{\omega}_z &= (F_{fxw}\sin(\delta) + F_{fyw}\cos(\delta))l_f - F_{ry}l_r \end{aligned} \quad (4.1)$$

**Constitution:**

$$F_{fyw} = -C_f s_{fy}; \quad F_{ry} = -C_r s_{ry}; \quad (4.2)$$

**Compatibility:**

$$s_{fy} = \frac{v_{fyw}}{|v_{fxw}|}; \quad s_{ry} = \frac{v_y - l_r \omega_z}{|v_x|}; \quad (4.3)$$

**Transformation from vehicle to wheel coordinate system on front axle:**

$$\begin{aligned} v_{fxw} &= (v_y + l_f \omega_z)\sin(\delta) + v_x \cos(\delta); \\ v_{fyw} &= (v_y + l_f \omega_z)\cos(\delta) - v_x \sin(\delta); \end{aligned} \quad (4.4)$$

As mentioned above, this model makes the following assumptions:

- Small tyre slip angle ( $\alpha_f$ ):  $s_{fy} = \tan(\alpha_f) \approx \alpha_f$ ;
- Small steer angle:  $\sin(\delta) \approx \delta$ ;  $\cos(\delta) \approx 1$ ;
- Small front body slip angle ( $\beta_f$ )  $\approx \frac{v_{fuv}}{v_{fxv}}$

Writing this equation in matrix form and neglecting longitudinal equilibrium (as we assume constant  $v_x$ , i.e.,  $\dot{v}_x = 0$ ) and it is also assumed that propulsive forces  $F_{fxw}$  and  $F_{fyw}$  to be neglected for lateral and yaw equilibrium:

$$\begin{bmatrix} m & 0 \\ 0 & J \end{bmatrix} \begin{bmatrix} \dot{v}_y \\ \dot{\omega}_z \end{bmatrix} + \begin{bmatrix} \frac{C_{12}+C_{34}}{|v_x|} & \frac{C_{12}l_f-C_{34}l_r}{|v_x|} + mv_x \\ \frac{C_{12}l_f-C_{34}l_r}{|v_x|} & \frac{C_{12}l_f^2+C_{34}l_r^2}{|v_x|} \end{bmatrix} \cdot \begin{bmatrix} v_y \\ \omega_z \end{bmatrix} = \begin{bmatrix} 1 \\ l_f \end{bmatrix} C_f \delta \quad (4.5)$$

**Linear bicycle model for tractor-semitrailer combination**

The model for a tractor semitrailer combination is very similar to the model derived above for a rigid-body vehicle [9]. First the model equations for the tractor unit is derived. The equations for longitudinal equilibrium shall be neglected, as above, since constant  $v_x$  is assumed. This model introduces the constraint forces  $P_{1x}$ ,  $P_{1y}$ ,  $P_{2x}$ ,  $P_{2y}$  between the tractor and semitrailer unit as well the articulation angle between tractor and semitrailer denoted by  $\theta$ . All other quantities have been explicitly been shown in figure 4.3.

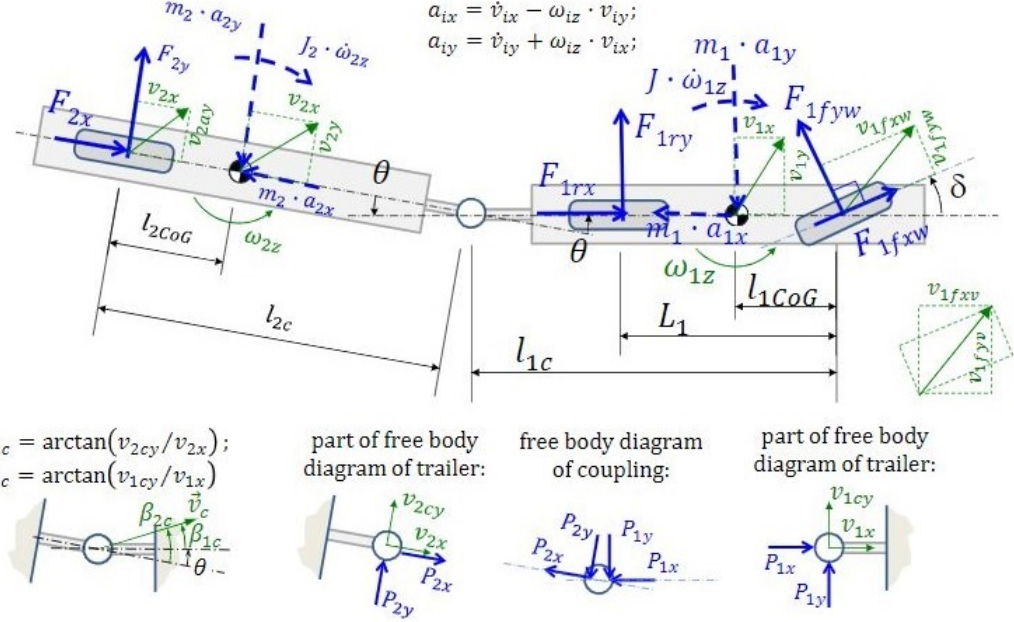


Figure 4.3: Bicycle model for two-unit articulated vehicle. Image Courtesy: Vehicle Dynamics Compendium, 2019 Edition [9]

#### Model equations for the 1<sup>st</sup> unit:

**Equilibrium of 1<sup>st</sup> unit (lateral, yaw around CoG):**

$$\begin{aligned} m_1(\dot{v}_{1y} + \omega_{1z}v_x) &= \sin(\delta)F_{1fxw} + \cos(\delta)F_{1fyw} + F_{1ry} + P_{1y}; \\ J_1\dot{\omega}_{1z} &= (\sin(\delta)F_{1fxw} + \cos(\delta)F_{1fyw})l_{1CoG} - F_{1ry}(L_1 - l_{1CoG}) + (-P_{1y})(l_{1c} - l_{1CoG}); \end{aligned} \quad (4.6)$$

**Constitution for axles on 1<sup>st</sup> unit:**

$$F_{1fyw} = -C_{1f}s_{1sy}; \quad F_{1ry} = -C_{1r}s_{1ry}; \quad (4.7)$$

**Compatibility within 1<sup>st</sup> unit:**

$$\begin{aligned} s_{1sy} &= v_{1fyw}/|v_{1fxw}|; \quad s_{1ry} = v_{1ry}/|v_x|; \\ v_{1fxw} &= \cos(\delta)v_x + \sin(\delta)v_{1fyw}; \\ v_{1fyw} &= -\sin(\delta)v_x + \cos(\delta)v_{1fyw}; \\ v_{1fyw} &= v_{1y} + \omega_{1z}l_{1CoG}; \\ v_{1ry} &= v_{1y} - \omega_{1z}(L_1 - l_{1CoG}); \\ v_{1cy} &= v_{1y} - \omega_{1z}(l_{1c} - l_{1CoG}); \end{aligned} \quad (4.8)$$

**Model equations for the 2<sup>nd</sup> unit:**

**Equilibrium of 2<sup>nd</sup> unit(lateral, yaw around CoG):**

$$\begin{aligned} m_2(\dot{v}_{2y} - \omega_{2z}v_x) &= F_{2y} + P_{2y}; \\ J_2\dot{\omega}_{2z} &= -F_{2y}l_{2CoG} + P_{2y}(l_{2c} - l_{2CoG}); \end{aligned} \quad (4.9)$$

**Constitution for axles on 2<sup>nd</sup> unit:**

$$f_{2y} = C_2s_{2y}; \quad (4.10)$$

**Compatibility within 2<sup>nd</sup> unit:**

$$\begin{aligned} s_{2y} &= v_{2ay}/|v_x|; \\ v_{2ay} &= v_{2y} - \omega_{2z}l_{2CoG}; \\ v_{2cy} &= v_{2y} + \omega_{2z}(l_{2c} - l_{2CoG}); \end{aligned} \quad (4.11)$$

**Model equations for the coupling:**

**Equilibrium of coupling:**

$$\begin{aligned} P_{1x} + \cos(\theta)P_{2x} + \sin(\theta)P_{2y} &= 0; \\ P_{1y} - \sin(\theta)P_{2x} + \cos(\theta)P_{2y} &= 0; \end{aligned} \quad (4.12)$$

**Compatibility of coupling:**

$$\begin{aligned} v_x &= \cos(\theta)v_x + \sin(\theta)v_{2cy}; \\ v_{1cy} &= -\sin(\theta)v_x + \cos(\theta)v_{2cy}; \\ \dot{\theta} &= \omega_{1z} - \omega_{2z}; \end{aligned} \quad (4.13)$$

Thus, the model for a tractor semitrailer combination gives us a DAE system with 24 equations and 24 unknowns which proves to be very cumbersome to solve using simple symbolic tools (for eg., Symbolic Math Toolbox in MATLAB) as algebraic manipulations will generate huge expressions (hundreds of tokens) or in the worst-case, even fail. Thus, the above system of equations needs to be reformulated and hence approximations are introduced:

### Simplified model with approximations

The constraint forces  $P_{1x}$ ,  $P_{1y}$ ,  $P_{2x}$ ,  $P_{2y}$  between the tractor and semitrailer unit are neglected. Small angles ( $\delta$ ,  $\alpha_{ij}$  are assumed. Other new, but conceptually same assumptions can be made for this semitrailer combination: small articulation angle  $\theta$  and lateral tyre forces in 2<sup>nd</sup> do not affect the entire vehicle longitudinally ( $F_{2y}\theta = 0$ ).

**Equilibrium equations for 1<sup>st</sup> unit:**

$$\begin{aligned} 0 &\approx -m_1a_{1y} + F_{1fxw}\delta + F_{1fyw} + F_{1ry} + (F_{2y} - m_2a_{2y}); \\ 0 &\approx (F_{1fxw}\delta + F_{1fyw})l_{1c} + F_{1ry}(l_{1c} - L_1) - m_1a_{1y}(l_{1c} - l_{1CoG}) - J_1\dot{\omega}_{1z}; \end{aligned} \quad (4.14)$$

**Equlibrium for semitrailer unit:**

$$0 = -F_{2y}l_{2CoG} + m_2a_{2y}(l_{2c} - l_{2CoG}) - J_2\dot{\omega}_{2z}; \quad (4.15)$$

**Compatibility in coupling:**

$$\dot{\theta} = \omega_{1z} - \omega_{2z}; \quad (4.16)$$

To find compatibility relations that eliminate  $v_{2y}$ , the following differentiated compatibility equation is derived:

$$\dot{v}_{2y} \approx (\dot{v}_{1y} - \dot{\omega}_{1z}(l_{1c} - l_{1CoG})) - (v_{1y} - \omega_{1z}(l_{1c} - l_{1CoG}))\theta\dot{\theta} + v_x\dot{\theta} - \dot{\omega}_{2z}(l_{2c} - l_{2CoG}); \quad (4.17)$$

**Constitution for axles to eliminate lateral forces  $F_{1fyw}$ ,  $F_{1ry}$ ,  $F_{2y}$ :**

$$\begin{aligned} F_{1fyw} &= -C_{1f}s_{1fyw}; \\ F_{1ry} &= -C_{1r}s_{1ryw}; F_{2y} = -C_2s_{2y}; \end{aligned} \quad (4.18)$$

Eliminating the slips  $s_{1fyw}$ ,  $s_{1ryw}$ ,  $s_{2y}$  and expressing them in state variables:

**Compatibility:**

$$\begin{aligned} s_{1fyw} &\approx v_{1fyv}/|v_x| - \delta; \\ s_{1ry} &= v_{1ry}/|v_x|; \\ s_{2y} &= v_{2ay}/|v_x|; \end{aligned} \quad (4.19)$$

where  $v_{1fyv} = v_{1y} + \omega_{1z}l_{1CoG}$ ;  $v_{1ry} = v_{1y} - \omega_{1z}(L_1 - l_{1CoG})$  and  $v_{2ay} = v_{2cy} - \omega_{2z}l_{2c}$ ;  $v_{2cy} \approx v_{1cy} + v_{1x}\theta$ ;

## 5 Methods for side-slip estimation

This chapter discusses the different methods used to estimate side-slip. All of these are observer approaches, which means that they relate the unknown state variables to the measured variables. The different designs of the observer stated in this chapter have their individual pros and cons and thus the respective results of each of the methods has been compared and documented.

### 5.1 Kinematic observer based on the linear bicycle model

One method to understand vehicle behaviour is through the use of mathematical models, which describe the vehicle behaviour when certain parameters are fed into the model.

Tyre forces and moments are the main influencing factors in vehicle cornering. These two forces are in turn, influenced by interactions between tyre and road. The parameters which affect such interactions are tyre slip, vertical load and cornering stiffness. Other parameters which affect the vehicle cornering behaviour are yaw rate and wheelbase. The first method presented to estimate side-slip is by physically modelling a mathematical model based on the linear bicycle model [16].

#### 5.1.1 Estimating side-slip from the bicycle model

The equations for the bicycle model are formulated as shown previously in Equation 4.5:

$$\begin{bmatrix} \dot{x}_1 \\ \dot{x}_2 \end{bmatrix} = \begin{bmatrix} \frac{\partial v_y}{\partial x_1} & \frac{\partial v_y}{\partial x_2} \\ \frac{\partial \omega_z}{\partial x_1} & \frac{\partial \omega_z}{\partial x_2} \end{bmatrix} \begin{bmatrix} x_1 \\ x_2 \end{bmatrix} + \begin{bmatrix} \frac{\partial v_y}{\partial u} \\ \frac{\partial \omega_z}{\partial u} \end{bmatrix} u \quad (5.1)$$

$$\begin{bmatrix} \dot{x}_1 \\ \dot{x}_2 \end{bmatrix} = \begin{bmatrix} -\frac{C_{34}-C_{12}}{mv_x} & -\frac{v_x^2 m - l_r C_{34} + l_f C_{12}}{mv_x} \\ -\frac{l_f C_{12} - l_r C_{34}}{I_z v_x} & \frac{l_f^2 C_{12} + l_r^2 C_{34}}{I_z v_x} \end{bmatrix} \begin{bmatrix} x_1 \\ x_2 \end{bmatrix} + \begin{bmatrix} \frac{C_{12}}{m} \\ \frac{l_f C_{12}}{I_z} \end{bmatrix} u \quad (5.2)$$

In equations 5.1 and 5.2,  $\dot{x}_1 = v_y$  and  $\dot{x}_2 = \omega_z$ . Solving the above equations for  $v_y$ , using Cramer's rule, while considering  $\dot{x}_1 = \dot{x}_2 = 0$ , i.e., for steady-state, we get a model-based expression for vehicle lateral velocity as:

$$v_y^{mod} = \frac{v_x(l_r(l_f + l_r)C_{12}C_{34} - l_f C_{12}mv_x^2)}{(l_f + l_r)^2 C_{12}C_{34} + mv_x^2(l_r C_{34} - l_f C_{12})}. \delta \quad (5.3)$$

Generally, in most cases  $v_y \ll v_x$ , and hence small angle approximation can be applied to equation 5.3 without a large error resulting. The model-based side-slip is then given as:

$$\beta_y^{mod} \approx \frac{v_y^{mod}}{v_x} \quad (5.4)$$

Since this thesis focuses on defining the minimum and maximum bounds for estimated sideslip, the bounds were set by providing an offset of  $\pm 20\%$  to the cornering stiffness as follows:

$$\begin{aligned} C_{12,max} &= 1.2 * C_{12}; & C_{34max} &= 1.2 * C_{34}; \\ C_{12min} &= 0.8 * C_{12}; & C_{34min} &= 0.8 * C_{12}; \end{aligned} \quad (5.5)$$

### 5.2 Side-slip estimation by integrating lateral acceleration

This method is based on estimating lateral velocity, and subsequently side-slip, by integrating the lateral acceleration with respect to time. This method uses measurement data from the vehicle's inertial measurement

unit (IMU), which measures the lateral acceleration, yaw rate and longitudinal velocity. The kinematic equations for a rigid body's lateral motion are given by

$$a_y = \dot{v}_y + \omega_z v_x - \dot{\phi}_x v_z + g \sin(\phi_x) \cos(\theta_y) \quad (5.6)$$

where  $a_y$  is the lateral acceleration of the vehicle's CoG,  $v_x$ ,  $v_y$  and  $v_z$  are the longitudinal, lateral and vertical velocities of the vehicle's CoG.  $\phi_x$  and  $\theta_y$  are respectively the Euler roll angle and pitch angle.  $g$  is the acceleration due to gravity.  $\dot{\phi}_x$  and  $\omega_z$  denote the angular roll and yaw rate respectively.

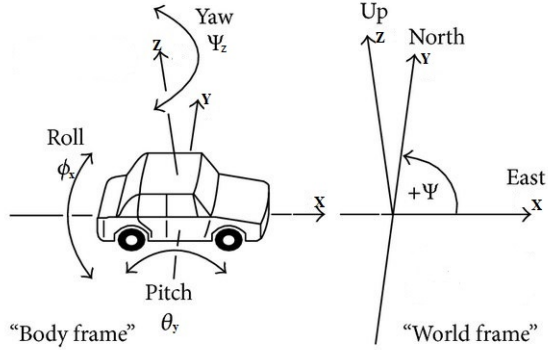


Figure 5.1: Roll, pitch and yaw angles for land-based vehicles.

The offsets required to define the minimum and maximum bounds, similar to the ones defined for the bicycle model have been introduced in this method. Bounds for the lateral acceleration in this method were defined based on real-world behaviour seen from measurement data, and thus an offset of  $\pm 5\%$  was introduced into the lateral acceleration as follows:

$$a_{y,max} = 1.05 * a_y; \quad a_{y,min} = 0.95 * a_y; \quad (5.7)$$

For small pitch angle and negligible  $v_z$ , the lateral velocity is approximately equal to

$$v_y^{kin} \approx \int_0^T (a_y - \omega_z v_x - g \sin(\phi_x)) dt \quad (5.8)$$

Assuming that body roll increases linearly with respect to lateral acceleration and neglecting road banking, we get the lateral velocity as:

$$v_y^{kin} \approx \int_0^T (a_y - \omega_z v_x - g \sin(\frac{a_y}{g} K_{roll})) dt \approx \int_0^T (a_y(1 - K_{roll}) - \omega_z v_x) dt \quad (5.9)$$

Here,  $K_{roll}$  is the vehicle roll gradient in [rad/g] and it is assumed that roll angle is small. By considering the minimum and maximum values of acceleration used to define the bounds as described in Equation 5.7, we get

$$\begin{aligned} v_{y,max}^{kin} &\approx \int_0^T (a_{y,max}(1 - K_{roll}) - \omega_z v_x) dt \\ v_{y,min}^{kin} &\approx \int_0^T (a_{y,min}(1 - K_{roll}) - \omega_z v_x) dt \end{aligned} \quad (5.10)$$

This method is vulnerable to the drift due to the presence of lateral sensor offset (also called accelerometer drift or integration drift). For this reason, the limitation of this method is that integration time must be short.

### 5.3 Washout filter method

A washout filter is a filter that makes a transition caused by changes in the input source more smooth. The side-slip estimated from the linear bicycle model is valid for steady-state manoeuvres and will cause errors when it comes to transient manoeuvres. The integration method, on the other hand is vulnerable to drift due to lateral sensor offset. Thus to counter the limitations of the two methods used above, it is possible to fuse information from both methods by using a washout filter where the low pass (LP) and high pass (HP) information can be retrieved according to:

$$v_y = LP(v_y^{mod}) + HP(v_y^{kin}) \quad (5.11)$$

We can see here that the lateral velocity from the bicycle model is low-passed and the lateral velocity from the integration methods is high-passed. Using a time constant  $T$  for the filter, the transfer functions of the HP and the LP filters are given as:

$$H_{LP}(s) = \frac{1}{1 + sT} \quad (5.12)$$

$$H_{HP}(s) = 1 - H_{LP}(s) = \frac{sT}{1 + sT} \quad (5.13)$$

Thus, equation 5.8 becomes

$$v_y = \frac{1}{1 + sT} v_y^{mod} + \frac{sT}{1 + sT} v_y^{kin} = \frac{1}{1 + sT} (v_y^{mod} + sT v_y^{kin}) \quad (5.14)$$

Substituting the value of  $v_y^{kin}$  from equation 2.7 into equation 2.11, we get

$$v_y = \frac{1}{1 + sT} (v_y^{mod} + T(a_y(1 - K_{roll}) - \omega_z v_x)) \quad (5.15)$$

This ends with a low-pass filter. The filter coefficient  $T$  is tunable, which determines the balance between the bicycle model and the measurement data.

# 6 Implementation

This chapter describes the implementation of the methods described in Chapter 5. The methods were implemented in MATLAB/Simulink so that it would enable the user to run the estimator for prototyping in a real vehicle for future testing. However, in this thesis, all the methods were executed offline on a personal computer. As mentioned in the previous chapter, there are three methods for implementing the state estimator which have been listed below.

## 6.1 Estimator using the bicycle model

The model, as shown in the figure, describes the lateral motion in steady state for a tyre to a road wheel angle  $\delta$ . The degrees of freedom for this model are the yaw and a component of lateral motion, with the corresponding state variables as lateral velocity  $v_y$  and yaw rate  $\omega_z$ . The vehicle longitudinal velocity  $v_x$  is assumed to be constant. This velocity was however, passed through a Low-Pass (LP) filter to smooth out disturbances in the measurements by choosing an appropriate filter constant. This model neglects the centre of gravity (CoG) height. The outputs of the MATLAB function block have three values for sideslip, namely, the maximum value,

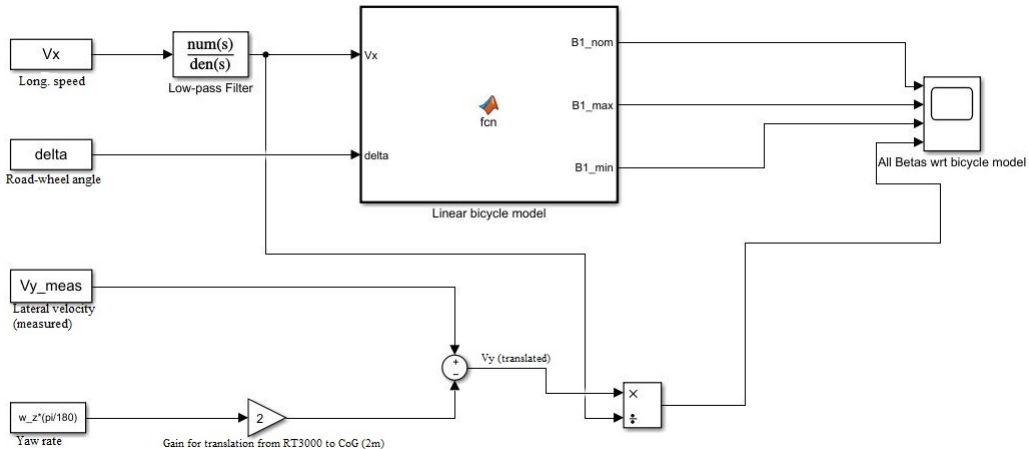


Figure 6.1: The Simulink model for a state estimator implemented using the bicycle model.

the nominal value and the minimum value. The min. and max. bounds were set by keeping an offset of  $\pm 20\%$ . This offset was chosen based on the tyre manufacturer's specifications for variation in tyre cornering stiffness due to regular wear and tear as well as reduction in tread depth. The estimated values were then plotted with the actual measured values from the RT3000 measurement system.

## 6.2 Model using the integration method

The bicycle model implemented in the previous section estimated the lateral velocity. The bicycle model is a physical model of the vehicle. Another method is to use kinematic relations and use measurements from the vehicle Inertial Measurement Unit (IMU), from which the vehicle's angular speeds and body accelerations are obtained. The lateral acceleration  $a_y$  which is fed as input is integrated with respect to time as elaborated using kinematic relations in Section 5.2.

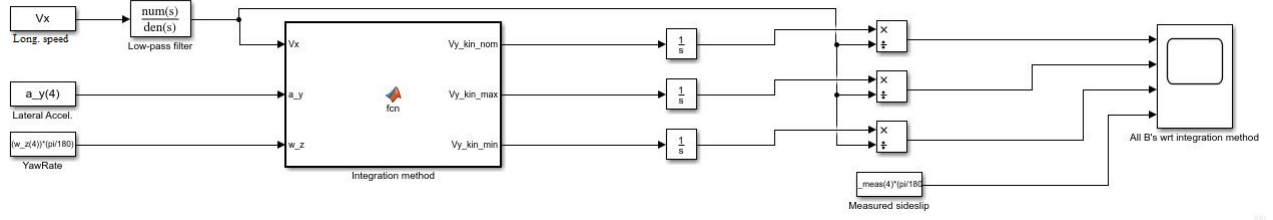


Figure 6.2: Simulink model for estimating sideslip by integrating lateral acceleration.

This method is the simplest of the three methods implemented. However, there is a gravity component, which contaminates the lateral accelerometer reading during non-planar motion. Thus, method becomes vulnerable to accelerometer drift (also called integration drift) which could lead to possible erroneous estimations for manoeuvres which have some degree of non-planar motion. The offsets which have been considered in the implementation of the Bicycle Model have been reused here, thus giving maximum, nominal and minimum values of lateral velocities, which in turn, give three values of vehicle sideslip. These estimated values are plotted against measured values of sideslip obtained from the RT3000.

### 6.3 Implementation of the washout filter

The description of the washout filter has been covered in Section 5.3. The model implemented in Simulink is shown below:

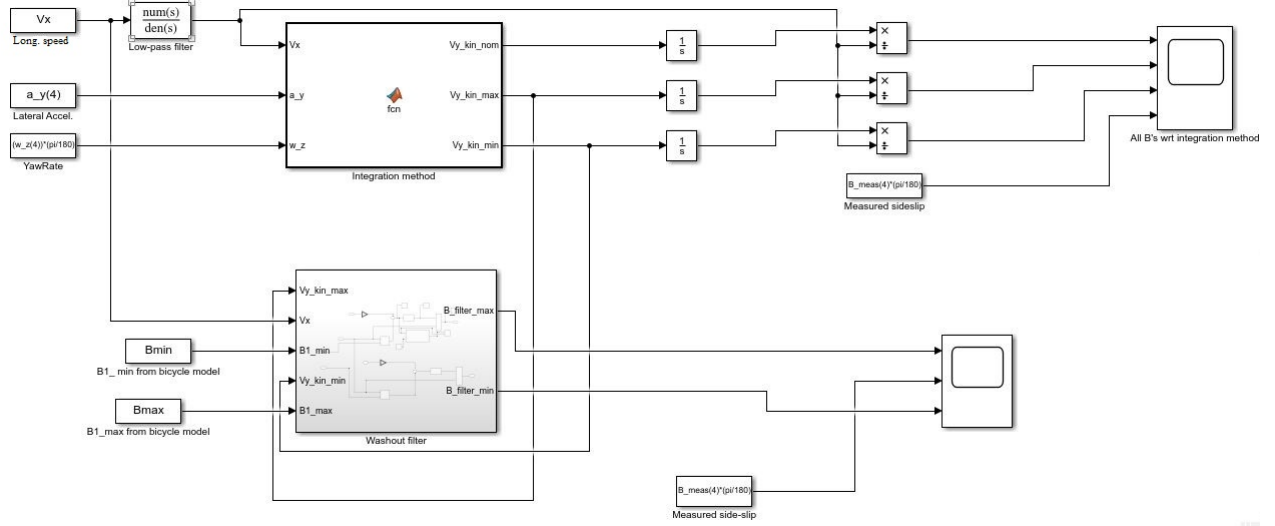


Figure 6.3: Simulink model for washout filter.

The washout filter uses the outputs obtained in both the previously described methods as inputs. In the previous methods mentioned above, the bicycle model is valid for steady state and gives fairly large estimation errors for transient manoeuvres, while the integration methods suffers from drift. The washout filter fuses the information from the two methods, thus retrieving the high pass and low pass information according to the expression in Equation 5.8.

The subsystem within the filter is described in the figure above. Although initially, the lateral velocity from the bicycle model is low passed and the lateral velocity from the integration method is high passed, we can

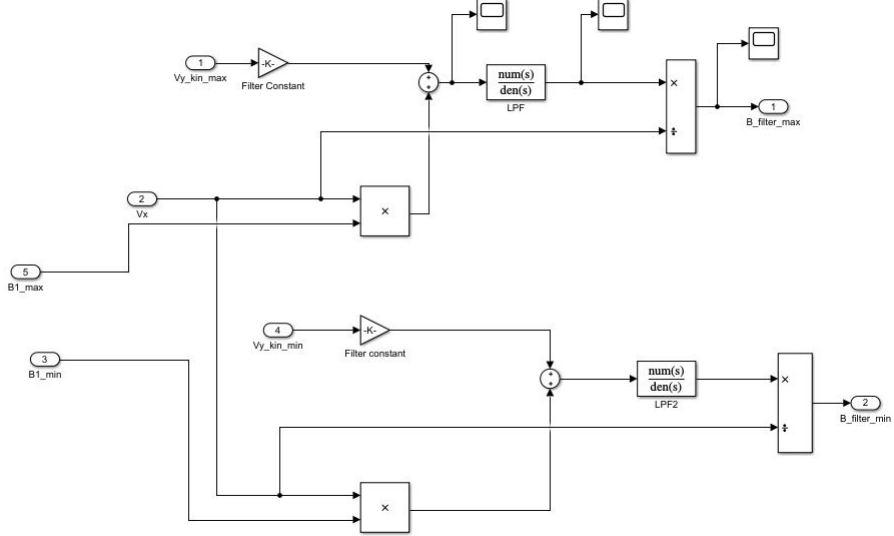


Figure 6.4: Model of subsystem which makes up the washout filter.

see from Equation 5.12 that the filtering equation ultimately ends with two low pass filters upon simplification which are shown in the subsystem, each having a filter constant  $T$  which can be tuned by trial-and-error to be valid for most transient manoeuvres. The manoeuvres considered in the scope of this thesis will be described more in detail in the sections to follow.

The washout filter acts as a special case of a Kalman Filter in the sense that it acts as a sensor fusion algorithm which fuses the information retrieved from the bicycle model method and the integration method and uses them as a priori while it uses the measured value of longitudinal velocity  $v_x$  as measurement data and combines them to predict the future estimated values of lateral velocity and thus, subsequently, sideslip. More in-depth details for the working and tuning of washout filters is given in [17].

## 7 Results and Analysis

This chapter describes the manoeuvres performed by a real vehicle (a Volvo FM series with a semitrailer combination) to obtain sensor data necessary for the state estimation in this thesis. The subsequent plots of estimated values versus measured values values are plotted for each of the three methods for the respective manoeuvres and the graphs are compared.

For the purpose of this thesis, originally five different manoeuvres were performed in varying road surface conditions (polished ice, non-polished ice and packed snow) as well as for different speeds. These were *Steady State Steering (small constant radius)*, *Steady State Steering (large constant radius)*, *Step Steering*, *Lane Change* and *Sinusoidal Steering (Slalom Manoeuvre)*. Focus was laid on three manoeuvres, namely the steady state steering (small constant radius), steady state steering (large constant radius) and the sinusoidal steering (slalom) manoeuvre.

### 7.0.1 Steady state steering with small constant radius

This manoeuvre was performed on non-polished ice to simulate a real-life scenario on slippery roads in winter. Data was logged for different speeds ranging from 15 km/h to 60 km/h with an increase in 5km/h after each data logging.

To get reasonably good estimates of sideslip, the data log for constant steady state steering at approximately 50 km/h (a relatively high speed) was considered as this give fairly measurable values of measured sideslip which would be easier to pictorially depict through graphs as compared to lower speeds. Given below is the trajectory of the path for the steady state steering manoeuvre in small circle.

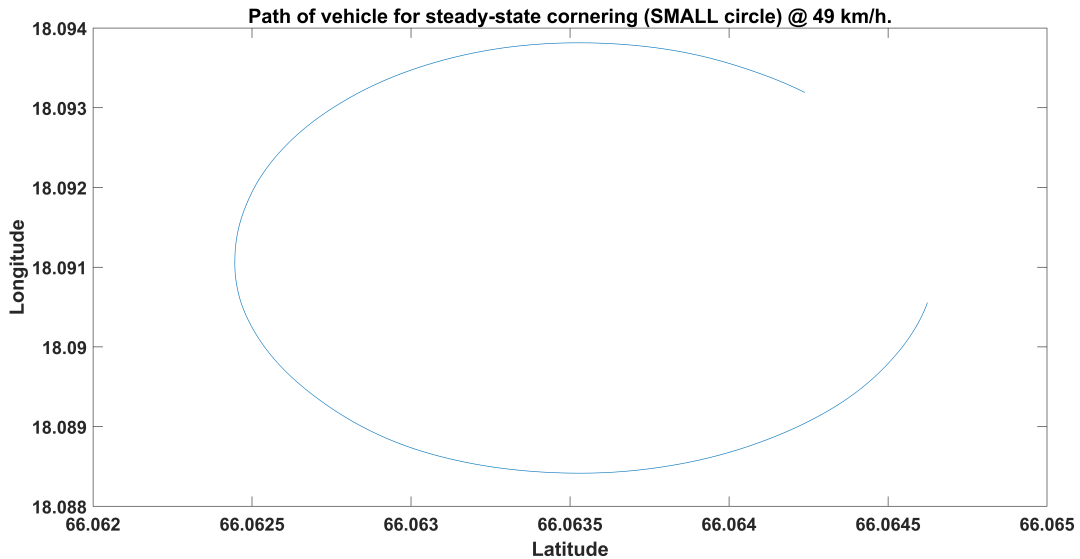


Figure 7.1: Path followed by vehicle for steady-state steering (small radius).

The graphs of estimated sideslip versus the measured values for the three methods are shown below:

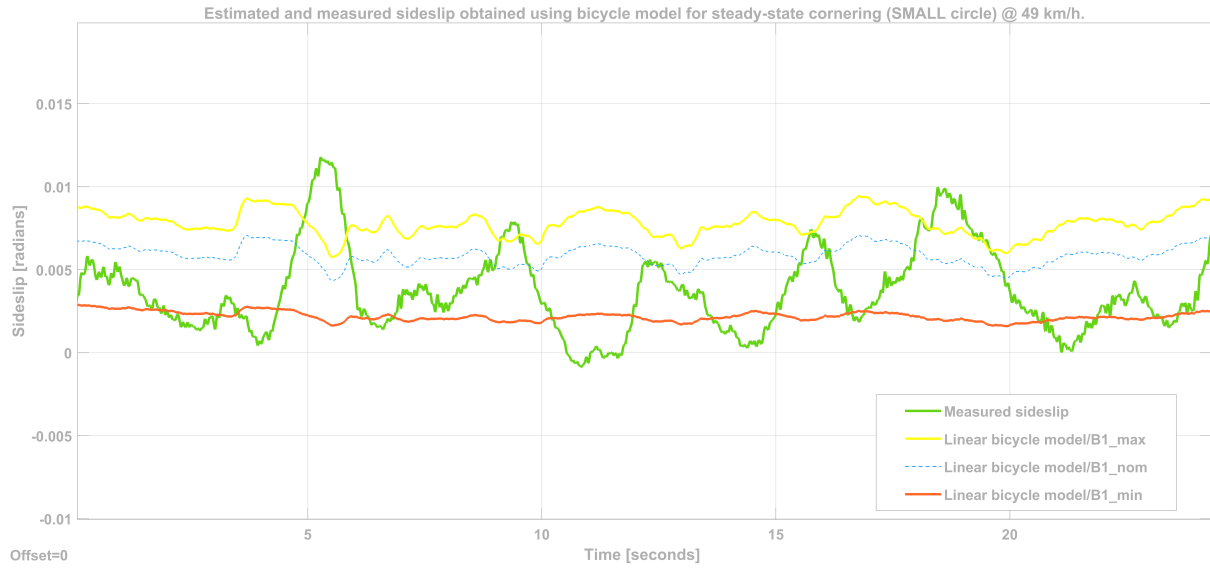


Figure 7.2: Estimated side-slip versus measured value using bicycle model for steady state cornering with small radius.

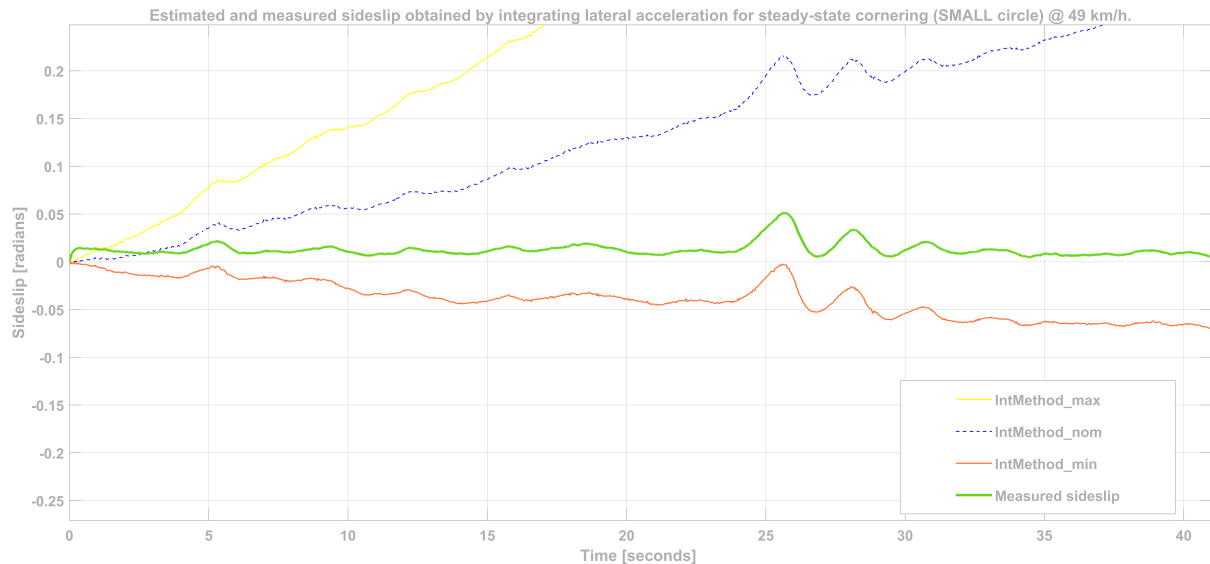


Figure 7.3: Estimated side-slip versus measured value by integrating lateral acceleration for steady state cornering with small radius.

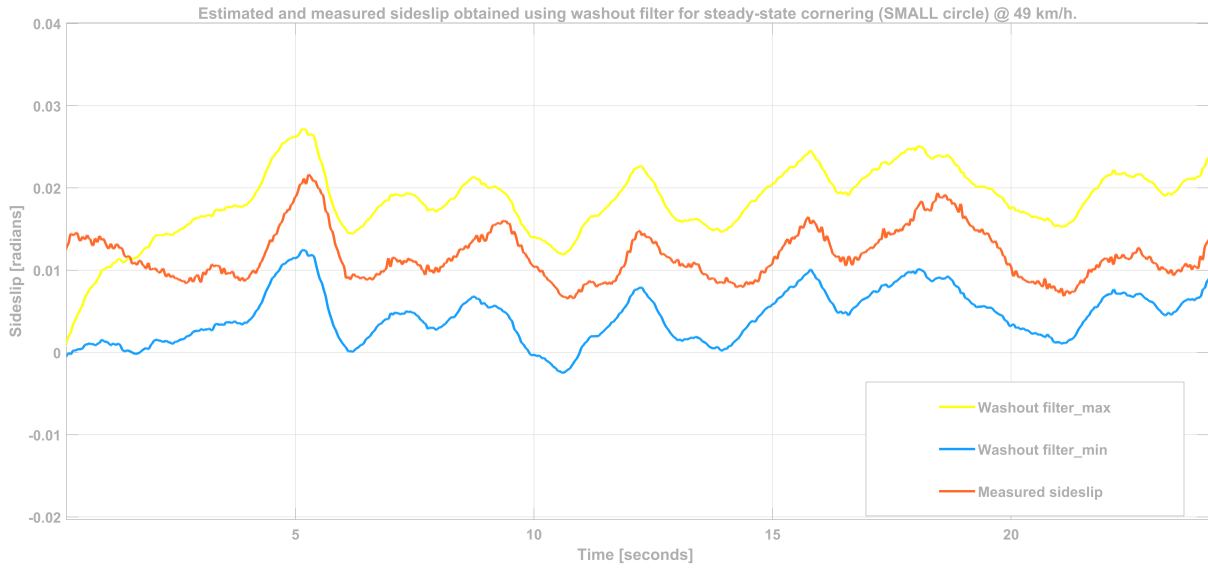


Figure 7.4: Estimated side-slip versus measured value using washout filter for steady state cornering with small radius.

In Figure 7.4, it can be seen that while the measured sideslip starts from a non-zero value (which in reality, is the case), the estimated values of minimum and maximum sideslip initially take some time to converge to the correctly estimated value and hence, at time  $t=0$ , both the min. and max. values are equal to zero. As time progresses, the estimated values converge to their more accurate value. The same is valid for Figures 7.8 and 7.12.

## 7.1 Steady state steering with large constant radius

This manoeuvre was performed similar to the previous manoeuvre with the slight differences being a larger radius of curvature and thus, higher speeds. Speeds from 30 km/h to 80 km/h with increments of 5 km/h were maintained and at each speed, the data was logged to give the measured value of the sideslip. Given below is the trajectory of the path for the steady state steering manoeuvre in large circle made at 50 km/h.

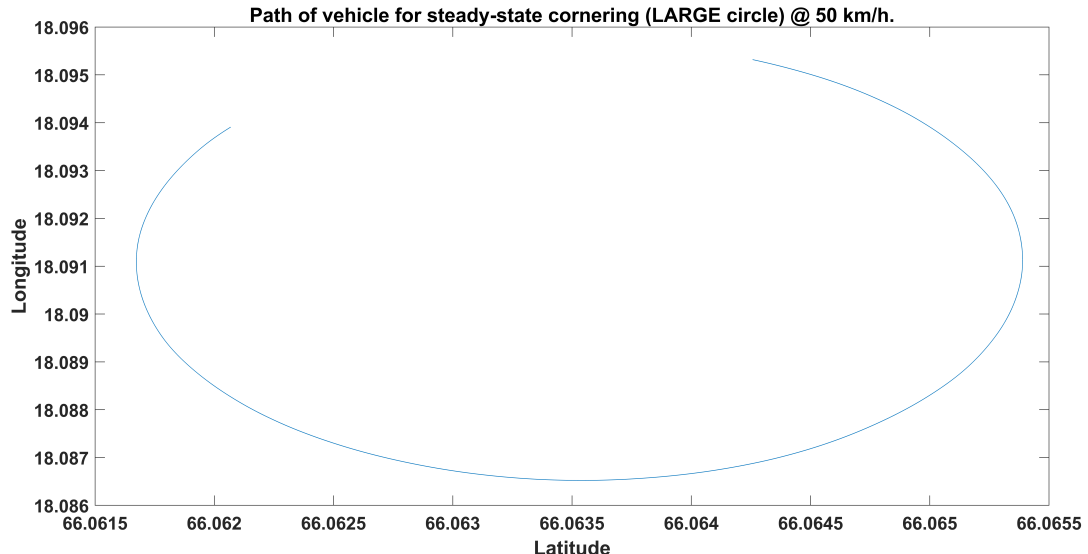


Figure 7.5: Path followed by vehicle for steady-state steering (large radius).

The graphs of estimated sideslip versus the measured values obtained by the three methods for the large radius steady state steering manoeuvre are shown below:



Figure 7.6: Estimated side-slip versus measured value using bicycle model for steady state cornering with large radius.

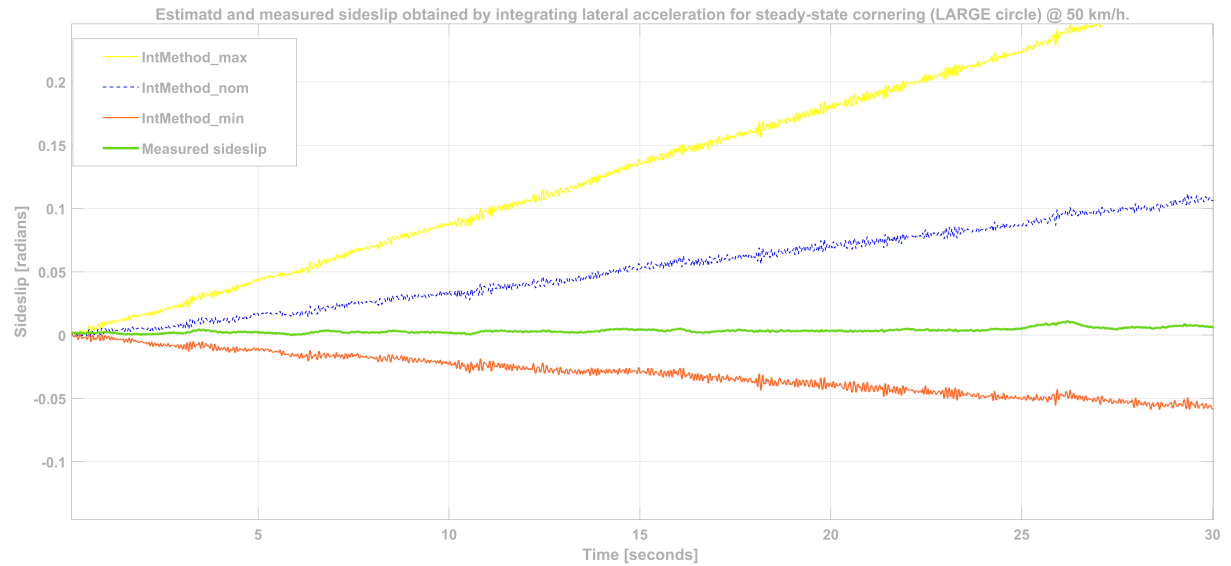


Figure 7.7: Estimated side-slip versus measured value by integrating lateral acceleration steady state cornering with large radius.

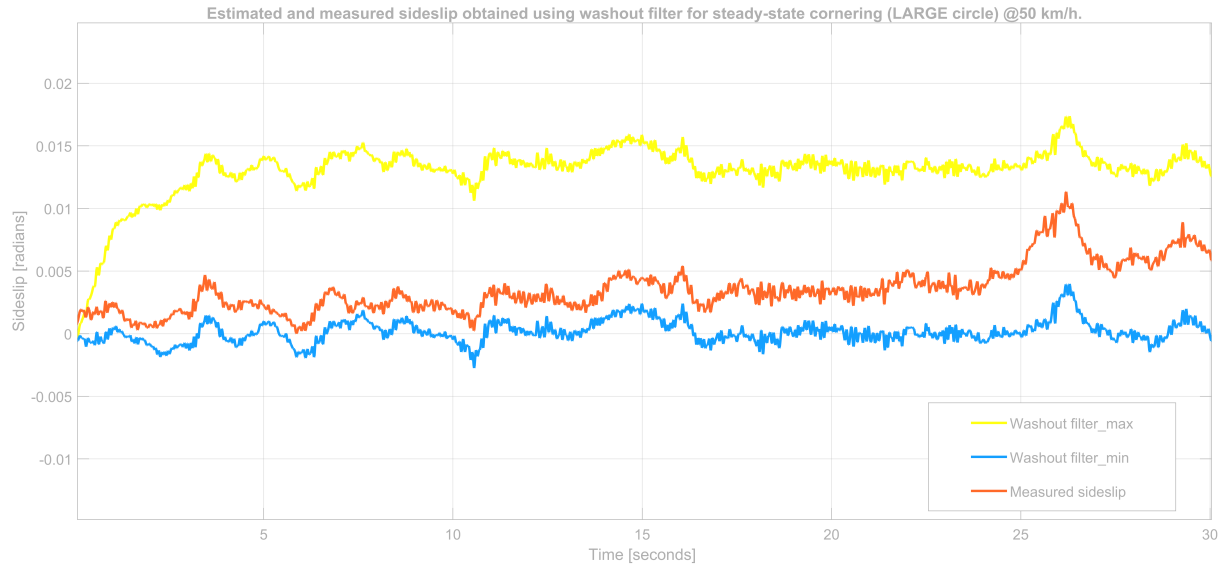


Figure 7.8: Estimated side-slip versus measured value using washout filter for steady state cornering with large radius.

The bicycle model and the method by integrating lateral acceleration give small estimation errors for above two manoeuvres, both of which maintain a steady state while cornering. The washout filter, on the other hand, gives reasonably good estimates of sideslip. As seen from the graph for washout filter, the measured value of sideslip lies within the min and max. bounds which have been defined previously.

## 7.2 Sinusoidal steering (slalom) manoeuvre

The slalom is basically a zigzag manoeuvre made by the vehicle in quick succession. This manoeuvre was performed on non-polished ice to simulate a real-life scenario on slippery roads in winter. Data was logged for three different speeds of 30 km/h, 50 km/h and 70 km/h. To maintain uniformity in speed with the previous two manoeuvres, the data log for the slalom manoeuvre made at 50 km/h was chosen.

This manoeuvre differs from the previous manoeuvres in the sense that this is a transient manoeuvre as compared to the steady-state steering manoeuvres described in the previous sections. There is a rapid change in the road-wheel angle of the vehicle along with rapid changes in direction in which the vehicle is headed along with rapid changes in values of measured sideslip, thus making accurate sideslip estimation all the more challenging. Since the path made by the vehicle, in its entirety, is approximately 1.4 km long, and the zigzag pattern made by the vehicle is a few metres at the maximum, it is very difficult to precisely show the zigzag pattern in the trajectory of the path made by the vehicle. Hence, it is chosen to show a parameter, the front road-wheel angle, a more easily depictable measure, which gives the reader a reflection of the path made by the vehicle in this manoeuvre.

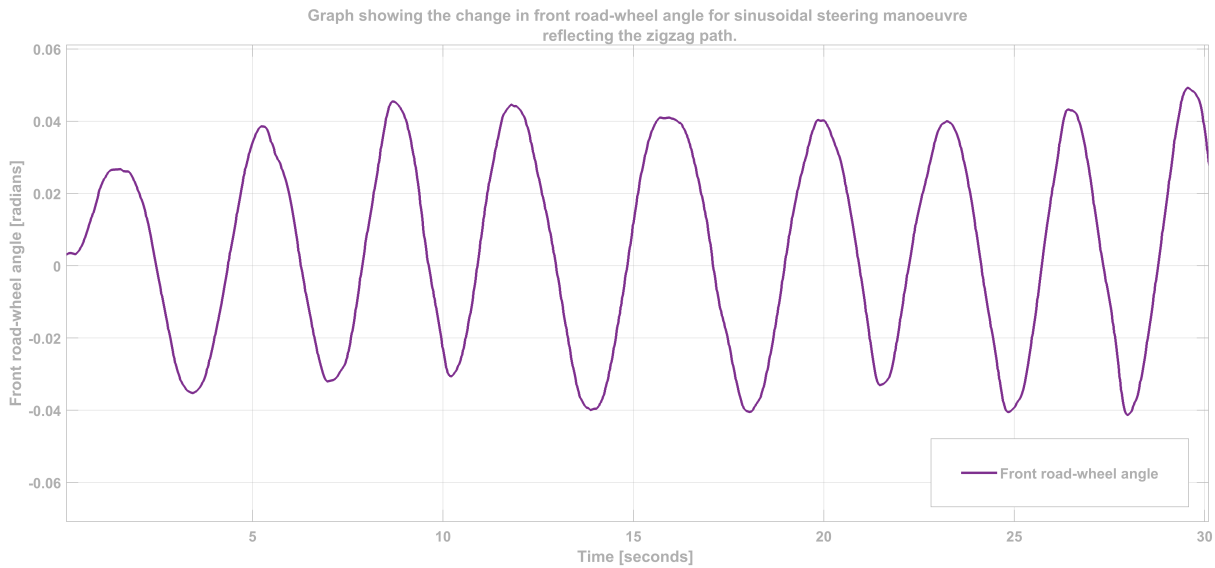


Figure 7.9: Change in front road-wheel angle for sinusoidal steering manoeuvre, showing a reflection of its path.

The graphs of estimated sideslip versus the measured values obtained by the three methods for the sinusoidal steering manoeuvre are shown below:

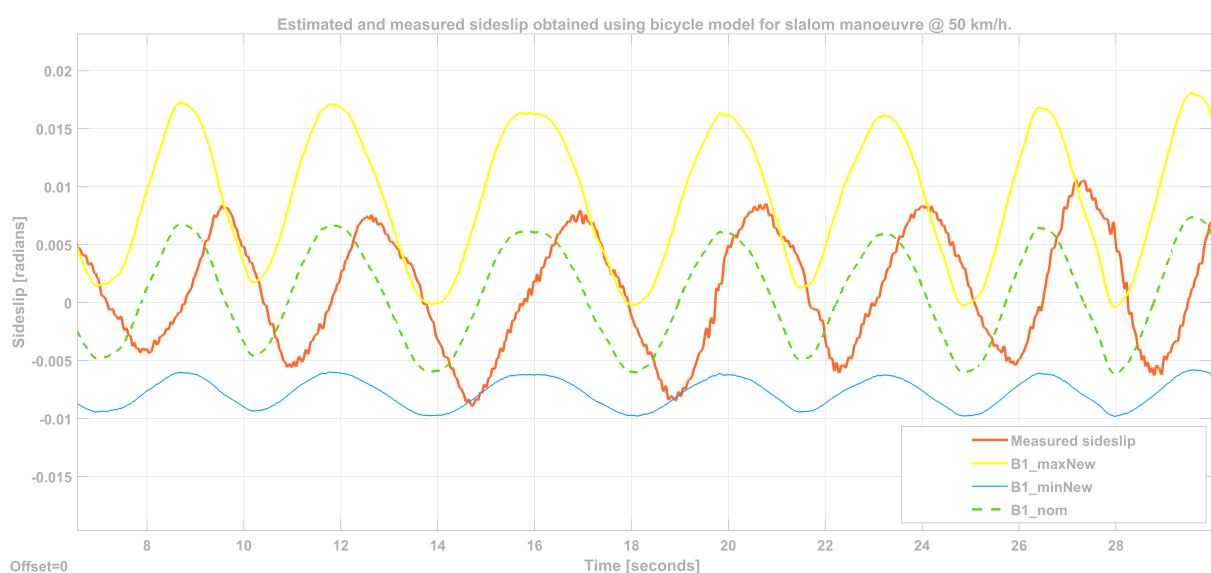


Figure 7.10: Estimated side-slip versus measured value obtained using the bicycle model for sinusoidal steering manoeuvre at 50 km/h.

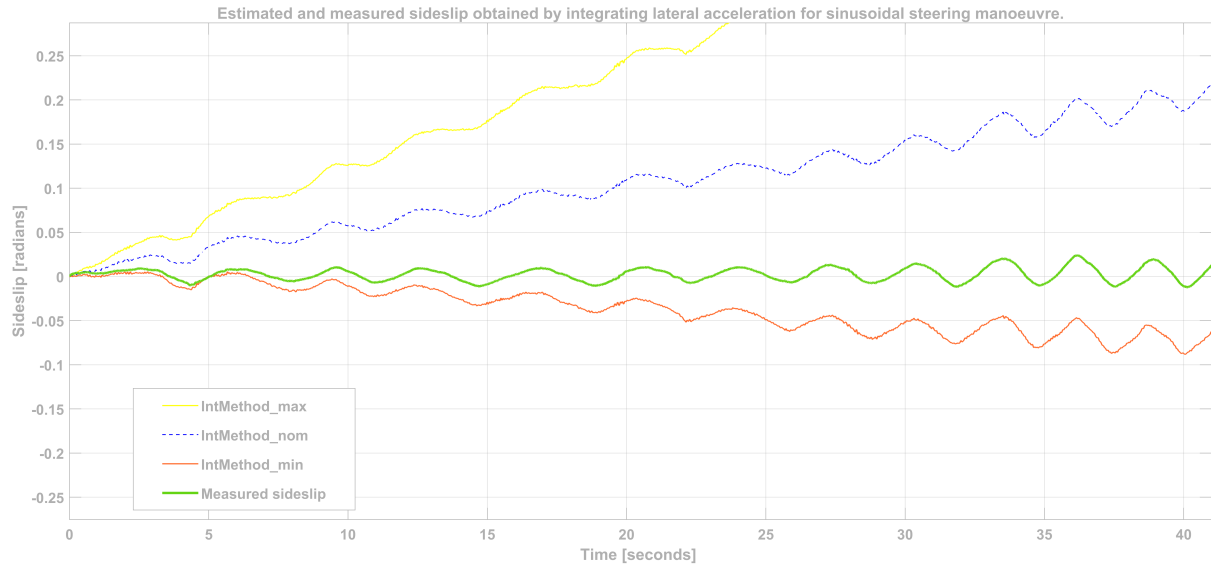


Figure 7.11: Estimated side-slip versus measured value obtained by integrating lateral acceleration for sinusoidal steering manoeuvre at 50 km/h.

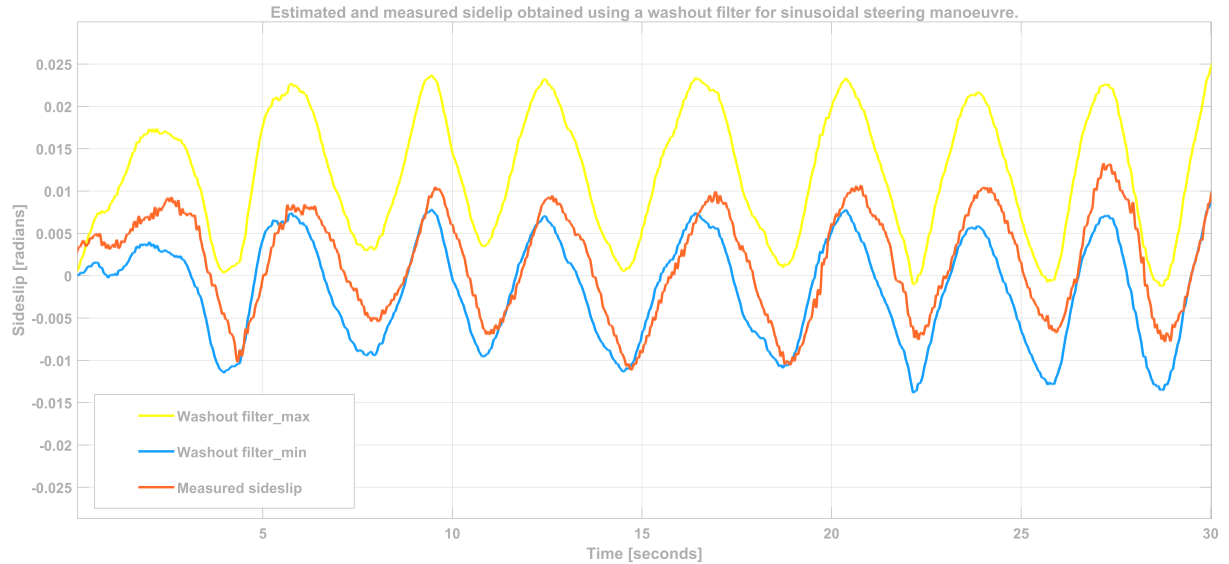


Figure 7.12: Estimated side-slip versus measured value using washout filter for sinusoidal steering manoeuvre at 50 km/h.

For transient manoeuvres such as this, the original graph for the bicycle model gave erroneous values of sideslip which frequently kept escaping the defined bounds. Also, since the slalom manoeuvre was a sinusoidal one, the physical nature of the bicycle model method meant that the graph of the minimum sideslip value showed a significantly smaller amplitude as compared to the graph of maximum value and the measured value. Therefore, there were instances in the sinusoidal pattern of the graph where the maximum value actually was below the minimum value. Hence, the bicycle model needed some modifications which ensured that the maximum always stayed above the minimum, and that there was always a non-zero distance between the minimum and maximum, at the cost of sacrificing some accuracy. The integration method, on the other hand, suffers from massive accelerometer drift. The washout filter maintains similar level of accuracy with the both the steady state manoeuvres as well as the transient manoeuvre and thus is the most reliable method which can be used to accurately estimate sideslip, regardless of the driving conditions.

## 8 Conclusion and future work

There have been many different approaches used over time for the estimation of vehicle sideslip, but most of them focus on passenger cars. This thesis focused on the estimation of sideslip for a heavy vehicle, namely a truck with a tractor semitrailer combination. Future works will need to consider larger and more complex combinations such as a full trailer, A double, B double or a dolly semitrailer. The estimation is based on measurements obtained from the *RT3000*, the vehicle IMU, together with the known vehicle geometry. This thesis has mainly focused on ensuring that the measured sideslip lies within the pre-defined bounds for minimum and maximum values of estimated sideslip. The aspect of computational complexity has not been emphasized on to a considerable extent.

### 8.1 Approach

The estimation methods implemented in this thesis are based on a complete vehicle model combined with the data from the inertial and GPS measurement system. Future research could incorporate further kinematic estimation strategies, such as an extended and a more complex bicycle model, as they are more robust to variations in vehicle parameters.

The bicycle model of the observer uses the Linear Tyre Model to describe the tyre forces up to and beyond the friction limit. Other models such as the Magic Formula, Brush Model or the Dugoff's Tyre Model which could effectively take into consideration the computational complexity could be considered in future research. Throughout the scope of this thesis, the road surface is assumed to be horizontal, and thus needs to be extended in order to describe the vehicle dynamics while driving on banked or inclined roads. Also, load transfer has been neglected, and will thus need to be considered in future works when considering multi-axle vehicles.

### 8.2 Implementation

The implementation of the three estimation method described in this thesis was made in MATLAB/Simulink. The bicycle model and the washout filter have been implemented as separate Simulink blocks, allowing them to be used independently as and when required. This method of implementation enables the user to easily modify or replace parts of the model. Some known errors exist in the implementation, which need to be addressed for future use.

### 8.3 Accuracy

All of the estimation methods produced accurate estimates of vehicle sideslip for manoeuvres with low to medium friction utilizations such as a steady state cornering manouevre and at different speeds. The measured values of the sideslip lie well within the bounds for such manoeuvres, which is the desired outcome of this thesis. For situations where the vehicle momentarily skidded due to the slippery conditions of the surface, the estimated sideslip produced errors and resulted in the measured data escaping the bounds. Nonetheless, the estimates followed the measurements closely.

However for manouevres with a slightly high friction utilization such as a sinusoidal steering manoeuvre (slalom), the estimation produced larger errors when methods based on a physical model, such as the bicycle model were used, as such a manouevre corresponds to a critical driving condition. Errors were higher for situation where the sideslip was very large, but the trajectory of the bounds generally had the same shape as the measured sideslip graph. Nonetheless, the washout filter method produced desirable estimates, even for complex manouevres like the slalom.

## 8.4 Errors and noise in measurement data

The measured values of different vehicle velocities, accelerations, including the measured value of sideslip, were corrupted by sensor noise and need to be filtered using a Low-Pass Filter to make the measurements more readable. The measured values also needed to be translated to the vehicle's Centre of Gravity as the *RT3000* was placed approximately 2 metres away from the CoG. As mentioned previously, the effects of road inclination and banking on sensor errors need to be considered in future works.

## 8.5 Robustness

Most of the errors seen in the estimators were caused by measurement errors and uncertainties in vehicle parameters. The washout filter was very sensitive to phase delays caused due to incorrect tuning of the filter constant  $T$ . The washout filter as well as the bicycle model were also very sensitive to errors arising due to incorrect translation of data to the vehicle's CoG. However, all the methods used in estimation of sideslip were seen to be very robust to changes in vehicle mass. This is a very good property which can be implemented for use in trucks, where large variations in load is very common.

## 8.6 Parameter identification

The developed estimation methods require a fairly accurate knowledge of the different vehicle parameters they are seen to be sensitive to. Sensor offsets, offset values used to define the minimum and maximum bounds need to be clearly and accurately defined as these affect estimations greatly. The centre of gravity position also needs to be known accurately.

Also, for each of the manoeuvres, it was necessary to check if the utilized friction exceeded the maximum possible friction as in cases where it held true, the estimators failed to produce highly accurate values of the sideslip as compared to the sudden large variation in the actual measured sideslip. Thus, it always is required to ensure that the utilized friction does not exceed the max. possible value as this would produce large non-linearities which the developed estimation methods would find difficult to handle.

## References

- [1] M. P. DaSilva, G Ayres, and W. G. Najm, Crash problem definition and safety benefits methodology for stability control for single-unit medium and heavy trucks and large-platform buses. *Tech. rep., U.S. Department of Transportation* 2009, 2009.
- [2] H. B. Pacejka, *Tire and Vehicle Dynamics (Second Ed.)* Elsevier, 2006, ISBN: 0-7680-1702-5.
- [3] H. Grip, L. Imsland, T. Johansen, J. Kalkkuhl, and A. Suissa, Vehicle sideslip estimation, *Control Systems, IEEE* **29** Nov. 2009, 36–52, Nov. 2009. DOI: 10.1109/MCS.2009.934083.
- [4] *Rt3000 inertial and gps measurement system, User manual*, Oxford Technical Solutions Limited, 2005. [Online]. Available: <https://support.oxts.com/hc/en-us/articles/115001155865-RT3000-Online-manual>.
- [5] A. Van Zanten, Bosch esp systems: 5 years of experience, *SAE International* May 2000, May 2000.
- [6] S. Solmaz and S. Baslamisli, A nonlinear sideslip observer design methodology for automotive vehicles based on a rational tire model, *The International Journal of Advanced Manufacturing Technology* **60** May 2011, May 2011. DOI: 10.1007/s00170-011-3587-9.
- [7] L. Wang and F. Wang, Intelligent calibration method of low cost mems inertial measurement unit for an fpga-based navigation system, *International Journal of Intelligent Engineering and Systems* **4** Feb. 2011, Feb. 2011.
- [8] *Iso 8855:2011(en) road vehicles — vehicle dynamics and road-holding ability*, International Organization for Standardization, 2011. [Online]. Available: <https://www.iso.org/obp/ui/#iso:std:iso:8855:ed-2:v1:en>.
- [9] B. Jacobsson, *Vehicle Dynamics Compendium for Course MMF062*. Chalmers University of Technology, 2018.
- [10] M. Arrambide and E. Durling, *Design of a side-slip observer for single-unit heavy trucks, master thesis*, 2010.
- [11] *Iso 26262-3:2011(en) road vehicles — functional safety — part 3: Concept phase*, International Organization for Standardization, 2011. [Online]. Available: <https://www.iso.org/obp/ui/#iso:std:iso:26262:-3:ed-1:v1:en>.
- [12] *Iec 61508 - functional safety of electrical/electronic/programmable electronic safety-related systems (e/e/pe, or e/e/pes)*, International Electrotechnical Commission. [Online]. Available: <https://www.iec.ch/functionsafety/>.
- [13] N. Instruments. (). What is the iso 26262 functional safety standard, [Online]. Available: <http://www.ni.com/en-us/innovations/white-papers/11/what-is-the-iso-26262-functional-safety-standard-.html>.
- [14] G. Baffet, A. Charara, and D. Lechner, Estimation of vehicle sideslip, tire force and wheel cornering stiffness, *Control Engineering Practice* **17**, no. 11 2009, 1255–1264, 2009, ISSN: 0967-0661. DOI: <https://doi.org/10.1016/j.conengprac.2009.05.005>. [Online]. Available: <http://www.sciencedirect.com/science/article/pii/S0967066109001129>.
- [15] H. Dugoff, P. S. Fancher, and L. Segel, An analysis of tire traction properties and their influence on vehicle dynamic performance, *SAE Transactions* **79** 1970, 1219–1243, 1970, ISSN: 0096736X, 25771531. [Online]. Available: <http://www.jstor.org/stable/44644491>.
- [16] *Lab 2 tutorial lateral dynamics - state estimation, Sd2231- applied vehicle dynamics control by mikael nybacka and mats jonasson*, KTH Royal Institute of Technology, 2014.
- [17] A. H. Munther and E. H. Abed, Generalized washout filters for control of nonlinear systems, *The Institute for Systems Research, University of Maryland*,